Numerical simulation for absorbing boundary conditions

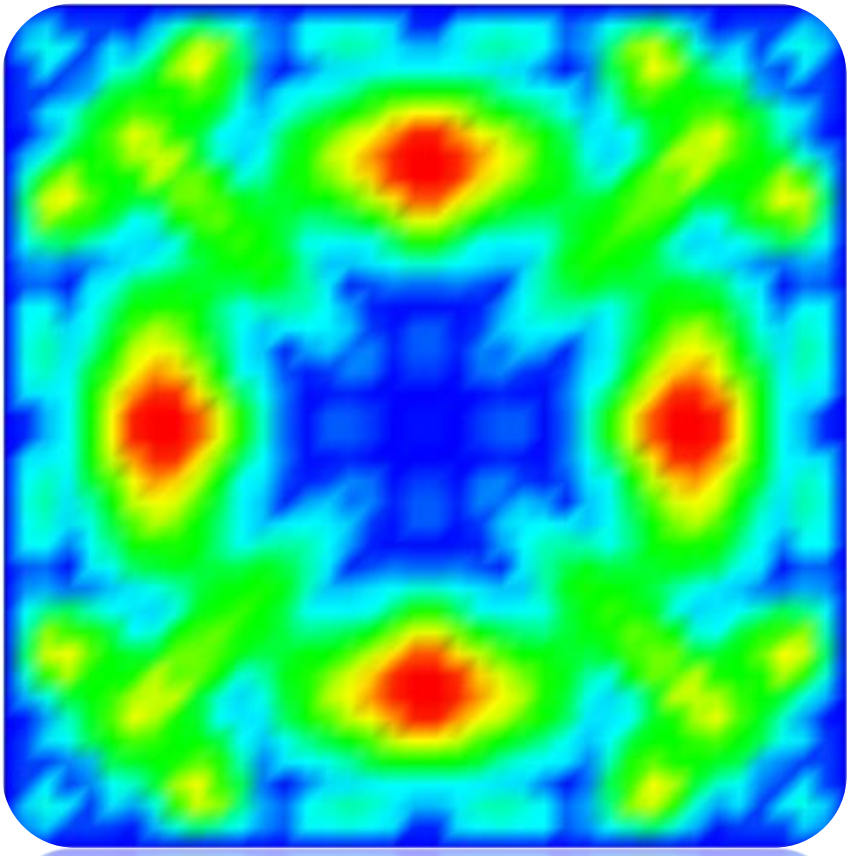

Vasko Kokalanov

September 2008

Ruhr University Bochum

ACKNOWLEDGMENTS

This was my first time to work with wave propagation and artificial boundary conditions and I am very thankful to my supervisor Prof. Dr. Vlatko Sesov, professor at the IZIIS institute in Skopje, who made it this work to be easier for me by guiding me with his knowledge through the problems.

I would like to thank Prof. Dr. Vlado Gicev, dean at the Faculty for Informatics in Stip, for several discussions and his advices from his reach practical experience, which were very helpful for completing the model in right way.

I am greatful to Dr. –Ing. Mathias Baitsch, scientific assistant at Faculty of civil engineering in Bochum, for supporting me with tools and advices about Java's Eclipse.

Finally, my sincerely thanks to my father, Prof. Dr. Gjorgi Kokalanov, professor at Faculty of civil engineering in Skopje, for the support and his help through the thesis and whole master coursel.

TABLE OF CONTENTS

LIST OF FIGURES

CHAPTER I
INTORDUCTION

1. Introduction

In many engineering and physics areas the problems which are investigated may be best represented or modeled by unbounded or semi - unbounded domains. The description of waves generated at shock producing industrial facilities or subway lines and their propagation through the soil, propagation of seismic waves and their approach toward the investigated objects, the propagation of noise generated by traffic route, the electromagnetic modeling of antennas, are only few topics that requires considering dynamics of infinite domains.

The key issue in modeling the dynamic behavior of infinite domains is the idea that there is no energy source at very large distance from the region being analyzed. All energy sources are circumscribed within a limited domain. So physically, energy generated at the bounded domains flows, usually as waves, from the source into the infinite domain and is not reflected. The unbounded domain is a perfect sink, where energy, in all its frequency and forms, is consumed.

Artificial boundary conditions (ABC) furnish a widely used approach for numerical treatment of boundary-value problems initially formulated on unbounded domains. These boundary conditions are typically set at the external boundary of a finite computational domain once the latter is obtained from the original unbounded domain by means of truncation. Implementation of ABC's enables to complete the "truncated problem" and therefore, makes this problem available for solution on the computer. However, to ensure well-posedness of the problem in the exterior, it must be supplied with the Somerfeld radiation conditions at infinity, which guarantee that the waves are purely outgoing and decaying as they approach infinity.

In the era of fast computers, obtaining solutions to many previously unsolvable problems became a reality, especially for problems involving partial differential equations (PDE), in which the analytical solutions exist only for the simplest condition. By utilizing numerical methods one can solve a problem from initial to some desired time at all spatial points. To solve a wave problem numerically in unbounded domain one usually introduces an artificial boundary, thereby defining a finite computational domain. On the artificial boundary one must impose some boundary conditions which should allow waves from the finite domain to pass through the artificial boundaries without generating spurious reflection.

The numerical solution of wave problems is a challenge common to many branches of engineering and applied mechanics. One aspect which must be considered when solving boundary value problems numerically, and which has both theoretical and computational importance, is the treatment of the boundary conditions. The choice of good physical boundary conditions for various problems and the way to combine this condition with the numerical scheme employed in the interior is an important subject of research.

1.2. Organization

This thesis is separated in two main parts. First one has two chapters while the second one has three chapters. In the first part the theoretical background of this work is presented, while in the second one consists the results and interpretation of the results. The two chapters in the theoretical part are Chapters II and III.

1. Chapter II begins with the idea of development the local and global artificial boundary conditions and goes on with a short review of some of the most important researches in field of artificial boundary conditions. In the last section of this chapter, it is given conclusions about the characteristics of global and local artificial boundary conditions.

2. Chapter III consists two main sections. The first one is describing the mathematical model, which will be used in the second section for deriving the finite difference scheme.

The results and the conclusions are given in the next three chapters

3. In Chapter IV first a review of the two most popular numerical methods is given, the Finite-Difference Method (FDM) and Finite Element Method (FEM). In the continuance are presented numerically and graphically the results obtained from the numerical model derived in the second section of Chapter III.

4. Chapter V is interpretation of the results represented in the previous chapter. In the discussions are stressed out the advantages and disadvantages of the experimented models.

5. In the last Chapter VI are given the conclusions about the Absorbing boundary conditions and whole model at all. In this chapter short recapitulation of the whole work is done. Additionally some ideas which are possible to apple such to obtain model applicable in practical problems or for further scientific researches.

CHAPTER II
ARTIFICIAL BOUNDARY CONDITIONS

2. Artificial boundary conditions (ABC): a review

For almost any problem formulated on an unbounded domain, there are, generally speaking, many different ways of closing its truncated counterpart. In other words, the choice of the ABC's is never unique. Clearly, the minimal necessary requirement of ABC's is to ensure the solvability of the truncated problem. If, however we restrict ourselves to this requirement only, then we cannot guarantee that the solution found inside the computational domain will be anywhere close to the corresponding fragment of the solution to the original (infinite domain) problem. Therefore, we must additionally require of the ABC's that the two solutions be in a certain sense close to each other on the truncated domain. An ideal case here would obviously be an exact coincidence of these two solutions, which leads us to formulating the concept of exact ABC's. Namely, we will refer to the ABC's as being exact if one can complement the solution calculated inside the finite domain to its exterior so that the original problem is solved. The concept of exact ABC's appears useful for the theoretical analysis of infinite domain analysis [1].

As the exact ABC's are not attainable routinely, the alternative is provided by various approximate local methods, which typically meet the other usual requirements of ABC's beside minimization of the error associated with the domain truncation. As mentioned above, these other requirements are low computational cost, geometric universality (i.e. applicability to a variety of irregular boundary conditions often encountered in real-life settings), and implementation without difficulties, in particular, readiness in combining the ABC's with the existing (interior) solvers.

Almost every numerical algorithm for setting the ABC's can be thought of as a compromise between the two foregoing groups of requirements that in a certain sense contradict one other. Shifting the balance towards locality and practical efficacy often implies insufficient accuracy; shifting it to the other side, towards high accurate nonlocal techniques, may often yield cumbersome and all but impractical algorithms.

In the following sections (2.1 and 2.2.) a review of different ABC's that have been published in the literature over recent years methodologies will be presented. One section will be dedicated for each, global and local boundary conditions.

2.1. Global methods

Engquist and Majda [3-4] one among the first who worked on ABC's, developed the time-dependent ABC's for some wave propagation problems, in particular those described by the wave equations and firs-order hyperbolic systems. Their approach is to represent the solution as a superposition of waves and to eliminate all incoming waves from the solution at the artificial boundary, because they can be interpreted as the reflection from the boundary. The ABC's that prohibit such waves are often called the non-reflected boundary conditions (NRBC's). This idea essentially implies that the exterior solution is sought for in the class of functions that can be composed of the outgoing waves only; this property constitutes the desired far-field behavior of the solution and can therefore be interpreted as the boundary condition at infinity; this boundary condition is then replaced by the ABC's at some finite artificial boundary.

Gustafsson [5] analyzed another hyperbolic problem, which from the standpoint of constructing ABC's is an additional complication. The initial data and the RHS source terms are no longer required to concentrate inside the computational domain (as by Engquist and Majda) but can also spread beyond the artificial boundary. The separation of variables using Laplace transforms in time and Fourier transform in space yield in this case in inhomogeneous relation that after the inverse transforms serves as nonlocal exact ABC at the planar artificial boundary.

Halpern [6] went further with his researches analyzing wider class of problems the so-called incompletely parabolic systems, i.e., the (small) higher-order parabolic-type perturbations of hyperbolic systems. A typical example of the system from this class is the Navier-Stoke equations for viscous fluid flows. In his work the ABC's for the linear half-space incompletely parabolic problem (planar Cartesian artificial boundary) are again obtained by first implementing the Fourier-Laplace transform and separating the variables and then explicitly selecting in the transformed space only those modes that comply with the desired behavior of the solution near infinity. Similarly to the boundary conditions from the previous authors [3-5], these boundaries can be approximated by some local relations.

Sofronov published series of papers [7-9] where he presented his technique for construction of exact three-dimensional ABC's for the wave equation as the spherical artificial boundary. Similarly to the works done from previous researches, the approach is also based on using the separation of variables. Spherical coordinates and Fouriers's expansion with respect to the spherical functions are employed in space; Laplace's transform is implemented in time. For the finite-difference formulation, the continuous spherical functions are substituted by the eigenvector of the discretized Beltrami operator on the sphere. These eigenvectors form an orthonormal basis and are called the difference spherical functions. The same type of approach has been carried out by Sofronov in later works (1995) for computation of the inviscid compressible flows in cylindrical wind tunnels. The inflow and outflow boundaries are planar cross-sections of the wind tunnel normal to its axis; the geometry and different governing Euler equations are linearized outside the computational domain. The resulting boundary conditions include the explicit formulas that connect the flow variables at the inflow and outflow artificial boundaries. An important part of the work by Sofronov is his approach to temporal localization of the exact ABC's.

Every one from the previous methodologies for exact ABC's (except first one by Sofronov) has strict limitations on the shape of the artificial boundary. The limitations are accounted for by the very nature of the techniques used for constructing ABC's; these techniques involve integral along the boundary and are essentially based on the separation of variables [1]. As way to achieve more geometric flexibility, Sofronov proposed first to enclose the actual artificial boundary (not essentially regular) between two additional spherical boundaries and the use interpolation. From the standpoint of geometry many local methods surveyed in Section 2.2 are much less restrictive. A highly accurate nonlocal ABC's methodology, which would at the same time be geometrically universal, can be calculated using difference potentials method.

One other direction in constructing ABC's was proposed by Givoli&Keller [10] by using the so-called Dirichlet to Neumann (DtN) mapping on the artificial boundaries. DtN relates the Dirichlet data u to the Neumann data $\frac{\partial u}{\partial n}$. First they construct the nonlocal exact ABC's for the Laplace equation and for some problems in elasticity. Further they developed similar boundary conditions for the Helmholtz equation, which is then solved by the finite elements method [11]. The approach is to express the normal derivative of the solution in terms of the solution itself so that the particular desired asymptotic of the solution at infinity is enforced. For the Helmholtz equation the Somerfeld radiation condition at infinity is enforced. They proved that combination of the exact boundary conditions with the finite

element method is very efficient. Also they are showing that the non-locality does not spoil the banded structure of the finite element matrix and does not increase the computation time significantly.

Practical implementation of the true exact ABC's for time-dependent problems presents more substantial difficulties compared to the steady-state case. The primary reason for that is the non-locality of the exact ABC's not only in space but in time. This non-locality may cause serve computational problems, mainly because when the numerical solution advance in time the amount of information to be stored in computer memory for updating the boundary conditions will need to constantly increase [1].

Givoli [12] generalized and extends the original DtN-based methodology to allow for the treatment of time-dependent problems. The idea consists analyzing the "steady-state" system that arises on the upper time level when one integrates the time-dependent problem by an implicit method. The resulting boundary conditions appear nonlocal in space and local in time; in this particular case the localization in time implies that the overall ABC's can be referred to only as approximated rather than exact [1].

Grote and Keller [13-14] proposed approach for temporal localization of the exact time-dependent ABC's. The study was made on three-dimensional wave equation outside a sphere and first they used expansion in spherical harmonic to reduce the problem to a family of one-dimensional "radial" equations with variable coefficients. The reciprocal of the special transform that involves both the unknowns and the independent variables is used to reduce each of these equations to a standard one-dimensional wave equation with respect to a few functions. Finally the same idea that the exterior solution should consist only the outgoing waves is used.

Harari and Hughes [15] and Grote and Keller [16] specially analyze the truncated DtN maps for the Helmholtz equation. Truncation means taking only a certain number of leading terms in the infinite Fourier series that represent the original map, it is often done when discretizing and implementing the DtN map in practice, for example, in the FEM framework. For the Helmholtz equation, this truncation may disturb solvability of the problem and/or result in non-uniqueness of the solution for higher modes, which is associated with the possible resonance of the complementary (interior) domain. These authors have proposed different recopies to avoid this undesirable phenomenon. The uniqueness is guaranteed if a sufficient number of terms are taken into account before the truncation, or if the Somerfeld radiation condition is imposed on higher modes at finite artificial boundary rather than at infinity.

Hagstrom et al. [17] construct and applied radiation boundary conditions of arbitrary order for wave propagation with subsonic convention in exterior problem. The construction is based on the progressive wave (or multipole) expansion of outgoing solutions. Using auxaliry functions defined only on the artificial boundary, problems associated with the use of high-order derivatives, as in the original Bayliss-Turkel formulation, are avoided.

Gachter and Grote [18] derived exact non-reflecting boundary conditions for time-harmonic elastic waves in three space dimensions. This condition holds on a spherical surface, which separates the computational domain from the surrounding unbounded region. It estaqblishes an exact relation between the displacement field and its normal tangential tractions, and thus defines a Dirichlet-to-Neumann map on the boundary. The modified DtN confition is used to remove the difficulties that arise when the exact DtN condition is truncated for use in computation.

Premrov and Spacapan [19] proposed an iterative method, which varies the tangential dependence of the local DtN operator in each computational step, by problems of wave reflection from the fictitious boundary. The problem occurs when solving the wave

equation in exterior domain using local low-order DtN map for computational procedures applied for a finite domain.

2.2. Local methods

The first obvious idea on how to obtain the local ABC's is to develop an approximation to the previously derived global boundary conditions.

The beginnings of the local methods are related with the work done by Lysmer and Kuhlenmeyer [20]. They introduced a general method through which an infinite system can be approximated by finite one introducing the viscous boundary conditions. The resulting model they have analyzed by use of Finite Difference Method (FDM). Their viscous boundaries have the following form:

$$\sigma = a*\rho*V_P*\dot{w}$$

$$\tau = b*\rho*V_S*\dot{u}$$

where σ and τ are the normal and the shear stress respectively, ρ is the mass density, V_P and V_S are P-waves and S-waves velocities respectively (calculated with the well known equations), $\dot{w}$ and $\dot{u}$ are the normal and tangential velocities respectively and a and b are dimensionless parameters.

They have made energy consideration, to show the ability of the viscous boundaries to absorb impinging energy from elastic waves. As a measure they have used the energy ratio as ration between the transmitted energy from the reflected waves and transmitted energy from incident waves. This ratio can be computed by the amplitudes A and B (unknown amplitudes from the reflected waves; for their computation they gave two linear equations as function of the incident angle θ) by considering the energy flow to and from a unit area of the boundary. The incident and the reflected energy respectively are:

$$E_i = \frac{1}{2s}\rho V_S \omega^2 \sin\theta$$

$$E_r = \frac{1}{2s}\rho V_S \omega^2 A^2 \sin\theta + \frac{1}{2}\rho V_S \omega^2 B^2 \sin\upsilon$$

So the energy ration becomes:

$$\frac{E_r}{E_i} = A^2 + \frac{sin\nu}{sin\theta} B^2$$

The maximal absorption of the boundaries is when a=b=1. The absorption cannot be made perfect over the whole range of incident angles by any choice of a and b. These boundaries defined with a=b=1 are 98.5% effective in absorbing P-waves. Because of that and because of its simplicity, it os nowadays often used in practical computations.

Using various asymptotic in the transformed space, one can develop rational (e.g. Taylor or Pede) approximation to these symbols, then the resulting boundary in physical variables become differential, i.e. local. This idea has been implemented by many authors for different problems.

The non-locality of the exact ABC's is typically caused by the fact that these boundary conditions in the transformed space contain special expressions that cannot be mapped into regular differential operators and give rise to the pseudodifferential operator instead. Engquist and Majda [3] developed a special technique based on pseudodifferential operators to obtain a sequence of local boundary conditions of increasing order.

$$\frac{\partial u}{\partial t} + \frac{\partial u}{\partial x}\Big|_{x=0} = 0$$

$$\frac{\partial^2 u}{\partial t^2} - \frac{1}{2}\frac{\partial^2 u}{\partial y^2} + \frac{\partial^2 u}{\partial x \partial t}\Big|_{x=0} = 0$$

The first one corresponds to Taylor approximation of the dispersion relation used in global methods ($\sqrt{\omega^2 - \eta^2} = \omega(1 + O\left({\eta^2}/{\omega^2}\right)$), and the second one to

($\sqrt{\omega^2 - \eta^2} = \omega(1 - \frac{1}{2}{\eta^2}/{\omega^2} + O\left({\eta^4}/{\omega^4}\right)$). The next member of the sequences obtained by Pade approximation of order $O(\eta^6/\omega^6)$.

Hagstrom [21] had shown that over finite intervals of time the sequence of Pade approximations used by Engquist and Majda converges to the original operator as the approximation order increase.

Based on the global boundary of Engquist and Majda [3-4], Engquist and Clayton [22] developed paraxial boundary conditions, which are widely used nowadays. This local boundary method will be later used in the model, so it will be detail described.

The high-order local boundary conditions can be presented as product of first-order terms as well. Taking typical wave equation $u_{yy} = u_{tt} - u_{xx}$ we can rewrite this formula in following manner

$$\frac{\partial^2 u}{\partial t^2} - \frac{1}{2}\frac{\partial^2 u}{\partial y^2} + \frac{\partial^2 u}{\partial x \partial t} = \frac{1}{2}\left(\frac{\partial^2 u}{\partial t^2} + 2\frac{\partial^2 u}{\partial x^2} + \frac{\partial^2 u}{\partial x \partial t}\right) = \frac{1}{2}\left(\frac{\partial u}{\partial t} + \frac{\partial u}{\partial x}\right)^2$$

which in fact is product of the first order terms from the sequence of [1]. With this kind of representation can be seen that second-order boundaries are completely absorbing only for waves which are traveling along x-axis (normal incidence). Higdon [23] has developed the idea of Engquist and Majda [1] that for any given angel of incidence $\alpha \neq \pi/2$ the second-order boundary will cause less reflection than the first-order. Using this viewpoint Higdon has promoted the multi-directional boundaries in the following form:

$$\prod_j (cos\alpha_j \frac{\partial u}{\partial t} + \frac{\partial u}{\partial x})\Big|_{x=0} = 0$$

The terms in this product dissolve only these two plane waves: $u = u(t-\cos\alpha_j x-\sin\alpha_j y)$ traveling in direction $(\cos\alpha_j, \sin\alpha_j)$, i.e. at the angle of incidence α_j to the boundary x=0; and the wave $u = u(t-\cos\alpha_j x+\sin\alpha_j y)$ traveling in direction $(\cos\alpha_j,-\sin\alpha_j)$, i.e. at the angle of incidence $-\alpha_j$ to the boundary x = 0. The pre-selected plane waves leave the computational domain and travels through the boundaries without any reflection, but for other waves they generally produce reflections. In certain case (see [23], the overall reflection coefficient can be lower than the one coming from the [1].

Bayliss and Turkel [24-25] introduced another group of local ABC's techniques that use the asymptotic form of the solution, named expansion boundaries, because their boundaries are based on expansion of outgoing pressure. The proposed methodology does not relate directly to local approximations of the previously constructed exact ABC's. This method, in comparison with the previous, does not require the explicit knowledge of the coefficients in the asymptotic expansion. In fact, Bayliss and Turkel did not use the asymptotic form of the solution directly to set the ABC's, they rather construct a set of

special local differential relations that identically cancel out a prescribed number of leading terms in the corresponding series[1]. Being applied at the artificial boundary, these relations provide for the approximate local ABC's.

Local ABC's equivalent to the truncated DtN maps are exact for an initially prescribed number of Fourier modes, after which the map is truncated. Givoli and Keller [26] proposed an artificial boundary and a finite difference algorithm for treating a spherical artificial boundary with a spherical grid. The authors used leap-frog finite difference scheme to solve three problems:

a) Time harmonic source in full space;
b) Scattering of flow frequency plane wave vertically impinging upon a spherical obstacle;
c) Radiation from a circular piston on a sphere

For all of the problems, the proposed algorithm gives accurate results.

One alternative idea for localizing DtN boundary proposed Givoli and Palatachenko [27]. Given a special form of local differential operator on the boundary (with first-order radial and high-order tangential derivatives), they optimize its initially undetermined coefficients so that in the sense of L_2 norm it provides for the best approximation of the original DtN map. The optimal NRBC's which they presented may be of low order, but still represents high-order modes in the solution. They showed that the previously derived localized DtN conditions are special case of the new optimal conditions. Two types of techniques were proposed: solution-independent and solution-weighted.

Givoli [28] presented alternative way construct high-order local ABC's with a symmetric structure and with only low (first- and second-) order spatial and/or temporal derivatives using AHOC (arbitrary high-order condition). This enables the practical use of ABC's of arbitrarily high-order. In the case of time-harmonic waves with finite element discretization, the approach yields a symmetric C^0 finite element formulation in which standard elements can be employed. The general methodology was presented for both, the time-harmonic case (Helmholtz equation) and time-dependent case (the wave equation).

In one of the recently published papers, Lee and Kallivokas [29] discussed the performance of the local second-order absorbing boundary condition of elliptical shape for scattering and radiation problems. Using the method of images, they extended the applicability of elliptically shaped truncation boundaries to semi-infinite acoustic media. For problems in either time- or frequency-domains, involving near-surface structures of elongated cross-sections, they showed that significant computational savings are attainable when compared with semi-circular truncation geometries.

2.3. Symmary

Each of the two main group artificial boundary conditions has advantages and disadvantages.

Most of the global ABC's replace the Sommerfeld radiation condition with DtN at the boundary. In their original formulation they involve high-order derivatives both in time and tangential direction, which means that for practical application they must be truncated and hence an error is introduced. Some of them, instead of truncation of the series, they reduce the order of the derivatives which requires additionally unknowns. Finally, the behavior of the boundary cannot be predicted in a case in which the incoming plane wave and the outgoing cylindrical wave are meeting at the boundary [2].

The nonlocal boundaries are exact absorbers but they are nonlocal, for steady-state in space and for time-dependent problems also in time and one must truncated to be usable in practical computation. The exceptions are rare and, as a rule, restricted to one-dimensional model examples [1]. Speaking about the practical computation, their non-locality may imply cumbersomeness and high computational cost. Because FE formulation is more flexible by non-rectangular shape than the FD schemes, these boundaries are more suitable for FE formulation.

The primary reason for using the local ABC's is that one can easily implement the local ABC's, included their combination with the interior solvers. Of course reducing their order will lead to numerical accuracy of the resulting solution to be lower than the one provided by the exact ABC's. As concerns practical algorithm issues (easiness in implementation), all foregoing approaches in constructing local ABC's provide an essential simplification of the numerical algorithm compared with the direct implementation of nonlocal ABC's, as well as substantial reduction in required computational domain [1]. Because of the requirement that the local ABC's be of some simple shape, or saying with other words be a coordinate surface which allows the separation of variables in the governing equations, they are mostly derived for rectangular shape. The error, which actually is the reflection from the boundary, is depended upon the distance from the excitation. Their exactness is improved with increasing the distance of the boundary to the source.

These ABC's are very popular in FD applications which involve rectangular domains and complicated outgoing fields with wide frequency ranges [2].

CHAPTER III
COMPUTATIONAL MODEL

3. Problem formulation

3.1. Mathematical model

In order to be proved the effectiveness of the artificial boundaries it was necessary to develop a model. The model is consisting of 2-D vertical medium, in rectangular shape 80m x 80m (see fig. 1). In each direction there are 40 points separated on equal distance of 2m. This part of the media should represent the truncated part of the whole media. For the medium it is assumed that it is homogenous and isotropic ground of one layer, with ground characteristics defined indirectly (see eq. 3.2.) by the shear v_s and compressional velocities v_p. The ratio between compressional and shear velocity is assumed to be $\sqrt{3}$ in all experimented models. At point (20, 20) an explosive source is applied.

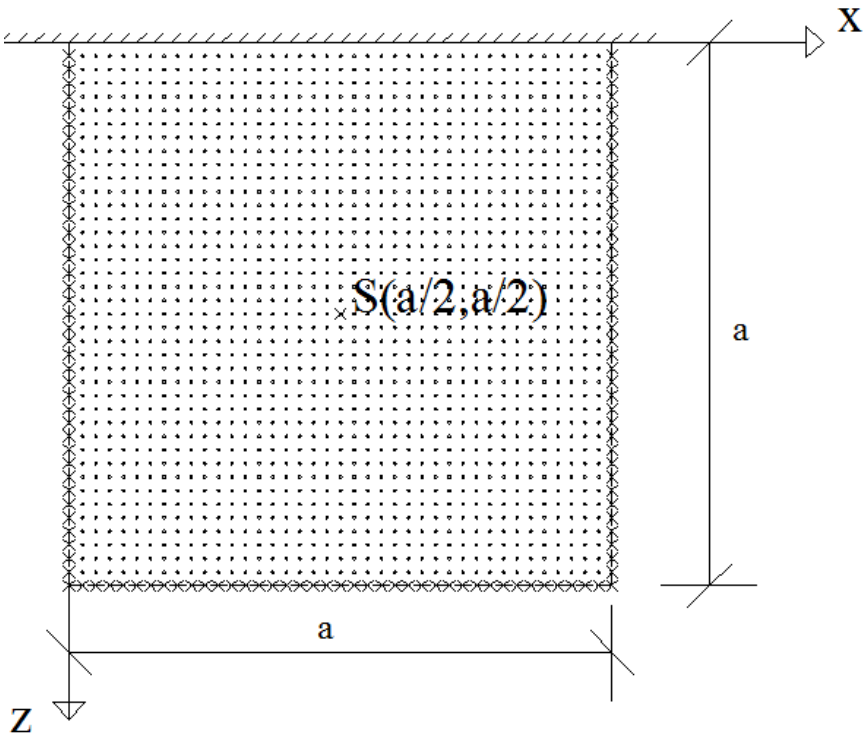

Figure 3.1 Test model

3.1.1. Equation of motion

In the model it is assumed that the horizontal axis is x axis, with positive values increasing from left to right, and vertical axis is z-axis, with positive values increasing downwards (see Figure 3.1). The starting point (0,0) is set on the upper left corner of the model. With this configuration two coupled, second-order, partial differential equation can be used to be described the motion of the P-waves and vertically polarized shear SV- waves [30]. The other shear waves, horizontally polarized SH-waves, are not included in the

analysis, because they are uncoupled from the previously mentioned P-waves and SV-waves. So the two equation of motion [31] in elastodynamic, describing the wave propagation are:

$$\rho \frac{\partial^2 u}{\partial t^2} = (\lambda + 2\mu)\left(\frac{\partial^2 u}{\partial x^2} + \frac{\partial^2 w}{\partial x \partial z}\right) + \mu\left(\frac{\partial^2 u}{\partial z^2} - \frac{\partial^2 w}{\partial x \partial z}\right)$$

$$\rho \frac{\partial^2 w}{\partial t^2} = (\lambda + 2\mu)\left(\frac{\partial^2 u}{\partial x \partial z} + \frac{\partial^2 w}{\partial z^2}\right) + \mu\left(\frac{\partial^2 w}{\partial x^2} - \frac{\partial^2 u}{\partial x \partial z}\right) \quad (3.1)$$

In this equation u and w are the horizontal and the vertical displacement respectively. Previously I have mentioned the density of the medium ρ and the Lame parameters λ and μ. The letter t is representing the time in the equations.

The velocities of the P-waves and S-waves, v_p and v_s respectively, are dependent on the ground characteristics and can be obtained by the following equations:

$$v_p = \sqrt{\frac{(\lambda+2\mu)}{\rho}}; \qquad v_s = \sqrt{\frac{\mu}{\rho}} \quad (3.2)$$

3.1.2. Initial conditions

At time t=0 it is assumed that there is no motion in the ground and hence the displacements u=w=0. Since the numerical model is explicit, which will be explained later (Section 3.2), two time steps are needed to be calculated the next one, it means that the displacements at time t=1 should be also prescribed. At t=1 I have supposed that only at the source point (See figure 2) the excitation is activated.

3.1.3. Boundary conditions

The infinite medium is made finite, and hence computational, by introducing the boundaries. Depending on the problem, different boundary conditions can be used on the edges: approximate-radiation conditions (representing infinite medium), stress-free conditions (also known as the Neumann conditions or free-surface conditions), or zero velocity conditions equivalent to zero-displacement conditions (known as Dirichlet boundaries on rigid surface) [32].

The internal interface between two layers with different soil parameters can be treated as boundary as well. Having in mind that they are in homogeneous formulation by treating explicit boundary conditions, they can be applied in mine model as well. But for simplicity of the model it is assumed medium from one layer.

In order to have more realistic model, for the upper boundary at level z = 0, a free surface boundary conditions. That means that the stresses must vanish on this boundary [33]:

$$(\alpha^2 - 2\beta^2)\frac{\partial u}{\partial x} + \alpha^2 \frac{\partial w}{\partial z} = 0$$

$$\frac{\partial u}{\partial z} + \frac{\partial w}{\partial x} = 0 \quad (3.3)$$

The other three boundary conditions (at x = 0; x = a and y = a) that were implemented in this model are based on paraxial approximations and one can find more about these

approximations in [3]. The authors of [3] presented a boundary condition which is non-local in both space and time. This boundary condition is impractical from a computational point of view since to advance one time level at a single point requires information from all previous times over the entire boundary [3]. And because of that they developed highly absorbing approximations and used those to build boundary which would be local and perfect absorbing.

The main feature of the paraxial approximations is that the outward-moving wave field can be separated from the inward-moving one. Along the boundary, the paraxial approximations can be used to model only the outward-moving energy and hence reduce the reflections. The boundary conditions are stable and computationally efficient in that they require about the same amount of work per mesh point for finite difference method as does the full wave equation [22].

The inventors of this boundary, Engquist and Clayton, in their paper [22] worked on the elastic wave equation in the following form:

$$\underline{u}_{tt} = D_1\underline{u}_{xx} + H\underline{u}_{xz} + D_2\underline{u}_{zz} \tag{3.4}$$

where :

$$\underline{u} = \begin{bmatrix} u \\ w \end{bmatrix} = \begin{bmatrix} vertical\ displacement \\ horizontal\ displacement \end{bmatrix}$$

$$D_1 = \begin{bmatrix} \alpha^2 & 0 \\ 0 & \beta^2 \end{bmatrix} \qquad H=(\alpha^2+\beta^2)\begin{bmatrix} 0 & 1 \\ 1 & 0 \end{bmatrix} \qquad D_1 = \begin{bmatrix} \beta^2 & 0 \\ 0 & \alpha^2 \end{bmatrix}$$

and α and β are the compressional and shear velocity respectively. They analyzed the following two paraxial approximations:

A1: $u_z + B_1u_t = 0$;

A2: $u_{tz} + C_1u_{tt} + C_2u_{tx} + C_3u_{tx} = 0$ (3.5)

The new three matrices which they introduced in the equations (3.4) are:

$$B_1 = C_1 = \begin{bmatrix} 1/\beta & 0 \\ 0 & 1/\alpha \end{bmatrix} \qquad C_2 = (\beta - \alpha)\begin{bmatrix} 0 & 1/\beta \\ 1/\alpha & 0 \end{bmatrix} \qquad C_3 = \frac{1}{2}\begin{bmatrix} \beta - 2\alpha & 0 \\ 0 & \alpha - 2\beta \end{bmatrix}$$

In Figure 3.2 the dispersion relations for the equations in (3.2) are shown. The fact that there are two curves for each approximations indicates that they decouple in to compressional and shear motions, as does the full wave equation. For the approximation A2, the shape of the dispersion curves depends on the ration of α and β, and the values in Figure 3.2 are obtained with the ratio $\sqrt{3}$, which will be used further in the model. In general, the larger the velocity ratio becomes, the poorer the approximations for shear waves [22]. In Figure 3.2 one can see the viscous boundaries of [20]. The curve is hyperbola independent of velocity ratio and indicates that the viscous boundaries will model shear waves less accurate than either A1 or A2 [22].

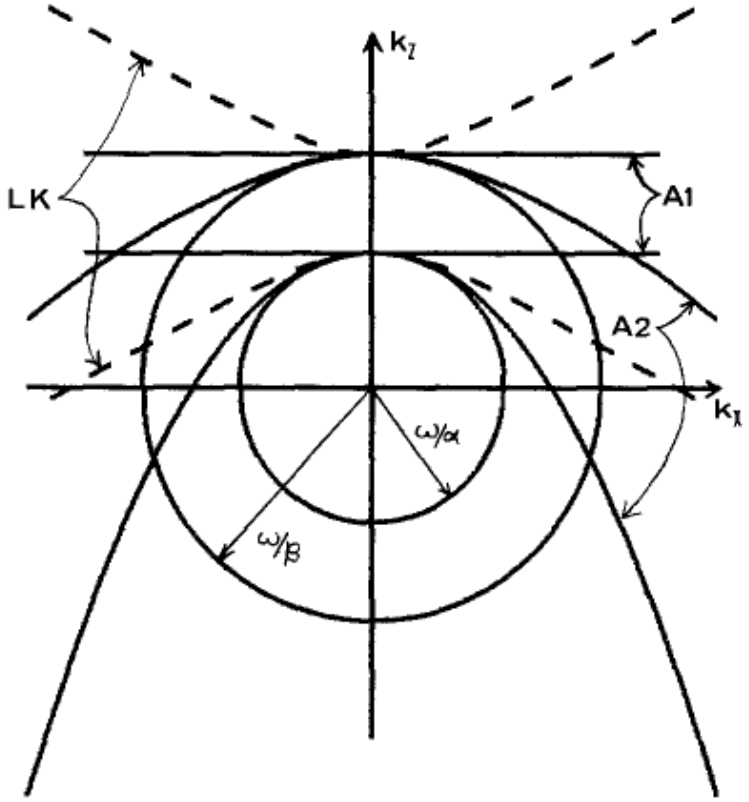

Figure 3.2 The curves A1 and A2 are the dispersion relations of the paraxial approximations of the elastic wave equation (the circles). For each approximation there are two curves: that approximating the larger circle is for shear wave while the other is for compressive waves. The dashed curves (labeled LK) are the dispersion curves of the viscous boundary conditions of Lysmer and Kuhlenmeyer [20]

The dispersion curves indicate that the paraxial approximations can be used to model elastic waves moving in one direction and to discriminate against waves moving in the opposite direction. To absorb incident energy along the boundary the paraxial approximations are used that models only the energy moving outward from the interior and grid toward the boundary.

A1 and A2 work for waves moving in positive z-direction, so this formulation will be suitable for the boundaries on level z = a. In case that absorbing boundaries are applied on the top as well, then it would have to be use the paraxial approximation with minus sign in the dispersion equation ($k_z = \pm(\omega/v)[1-(v^2k_x^2/\omega^2)]^{1/2}$). For the remaining two boundaries (x = 0 and x = a) are obtained only by interchange the x and z in the equations for top and bottom levels.

3.1.4. Source excitations

In order to generate the waves, an explosive source is used as excitation. The formulation for this kind of source, the Gaussian pulse, is as follows:

$$f(t) = e^{-\alpha(t-t_0)^2} \qquad (3.6)$$

where α is a parameter which controls the wave length content of excitation, t represents the actual time of calculation and t_0 is time when the function hits its maximum [32]. For Gaussian pulse the parameter is α = 3000 and maximum at time t_0 =0.036. At the maximum the Gaussian pulse has value equal to 1. By multiplication of f(t) with some factor one can vary the amplitude of the source. The multiplication factor for this model is 5 because such that bigger amplitudes are needed in order the model to be able to show effects like grid dispersion and the dumping in the model(see Chapter V). One important issue when one models explosive source is that the absolute value of the displacements must be equal in both direction $f_x(t) = f_z(t)$. The development of this function in time is given on the following figure:

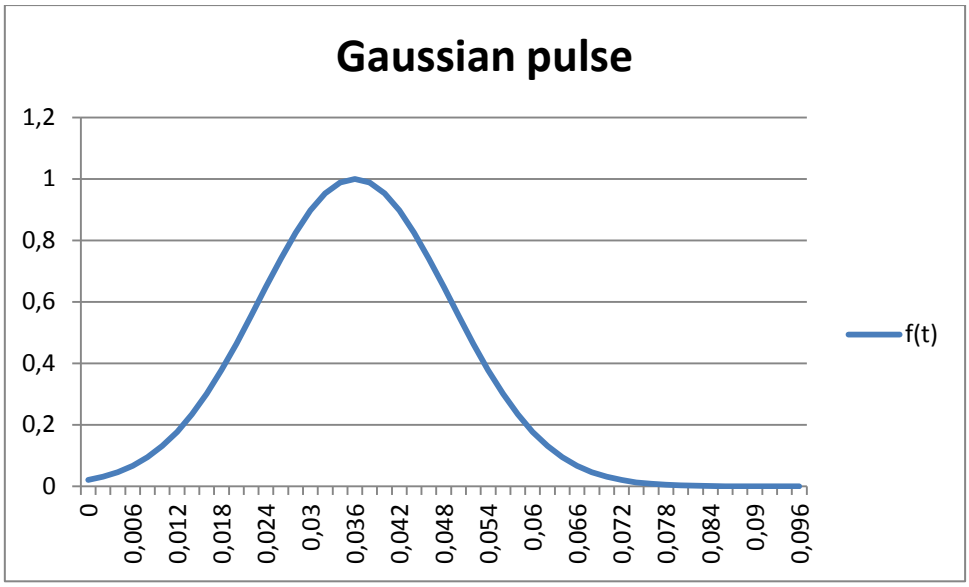

Figure 3.3 Displacement function f(t) in time

3.2. Numerical model

3.2.1. Numerical methods

Before the era of fast computers a lot of problems were unsolvable, especially problems defined by partial differential equations (PDE). Nowadays with the utilized numerical solutions one can solve a problem from initial time step to some desired time in all spatial points. Most frequently used numerical methods for solving the PDE's are finite element method (FEM) and finite difference method (FDM). FEM mostly use implicit methods, which means that the unknowns at all spatial points are obtained simultaneously for each time step by solving a system of linear algebraic equation. On the other hand, FDM is mostly based on explicit schemes, wherein the solution is obtained from the solution of the previous time step and the equations are uncoupled. So solving a full linear system of N^{th}-order leads to $O(N^2)$ operations for FEM and for uncoupled system by FDM the order of complexity is O(N). Hence, FDM is preferable for large-scale problems (N is big). Even the implicit schemes are usually symmetric and banded, which makes them smaller order then $O(N^2)$, they are still of higher order then explicit ones. When we speak about the numerical stability, the implicit schemes are unconditionally stable, what is not case for the explicit schemes. Being suitable for complicated and irregular shapes, gives advantage to FEM compared with the FDM. But for large-scale problems, as in seismological practice, the

explicit schemes are preferable because they are cheaper and easier to implement in numerical algorithms [2].

Knowing all mentioned positive and negative characteristics of both methods, and after some consultations with experienced people in this field, the conclusion was the model to be built by using FDM.

3.2.2 Equation of motion

In [30] Kelly has developed numerical model for the equations of motions (3.1). Same numerical approximation is used in the presented model to simulate the wave propagation in all grid points. So, using finite-difference numerical approximations Kelly according to the work of Ottaviani [34] presented the following coupled equations:

$$u(m, n, i+1) = 2*u(m, n, i) - u(m, n, i-1) +$$
$$+ F^2[u(m+1, n, i) - 2*u(m, n, i) + u(m-1, n, i)] +$$
$$+F^2(1-\gamma^2)[w(m+1, n+1, i) - w(m+1, n-1, i) - w(m-1, n+1, i) +w(m-1, n-1,i)] +$$
$$+ F^2 \gamma^2[u(m, n+1, i) -2*u(m, n, i) +u(m, n-1, i)]$$

$$w(m, n, i+1) = 2*w(m, n, i) - w(m, n, i-1) +$$
$$+ F^2[w(m, n+1, i) - 2*w(m, n, i) + w(m, n-1, i)] +$$
$$+F^2(1-\gamma^2)[u(m+1, n+1, i) - u(m+1, n-1, i) - u(m-1, n+1, i) + u(m-1, n-1,i)] +$$
$$+ F^2 \gamma^2[w(m+1, n, i) -2*w(m, n, i) + w(m-1, n, i)] \quad (3.7)$$

where x=mh, z=nh and t=iΔt. Δt is the time step and h is the grid interval in both x- and z-directions. Furthermore $\gamma=v_s/v_p$, where v_s and v_p are the velocities given with the equations (3.2). The parameter F can be calculated by:

$$F = \frac{v_p \Delta t}{h}$$

This parameter will be further used in stability calculations (see Section 3.2.5).

3.2.3. Boundary conditions

3.2.3.1 Absorbing boundaries

For the second-order elastic horizontal boundary conditions, related to equations (3.5) Clayton and Engquist propost the following formulation of finite difference scheme:

Bottom (n = a)

$$D_{-}^{z}D_{0}^{t}\ \underline{u}(m, a, i) + \frac{1}{2}C_1 D_{+}^{t}D_{-}^{t}\ (\underline{u}(m, A, i) + \underline{u}(m, a\text{-}1, i)) +$$

$$+ \frac{1}{2}C_2 D_{+}^{t}D_{0}^{x}(\underline{u}(m, a, i\text{-}1) + \underline{u}(m, a\text{-}1, i)) +$$

$$+ \frac{1}{2}C_3 D_{+}^{x}D_{-}^{x}\ (\underline{u}(m, a, i\text{-}1) + \underline{u}(m, a\text{-}1, i+1)) = 0$$

For the vertical boundaries the boundaries from Fuyuki and Matsumoto [35] are implemented, which are actually the same boundaries from [22] but in correct written form:

Left side (m = 0)

$$D_{+}^{x}D_{0}^{t}\ \underline{u}(0, n, i) - \frac{1}{2}C_1' D_{+}^{t}D_{-}^{t}\ (\underline{u}(0, n, i) + \underline{u}(1, n, i)) +$$

$$+ \frac{1}{2}C_2^{T} D_{+}^{t}D_{0}^{z}\ (\underline{u}(0, n, i\text{-}1) + \underline{u}(1, n, i)) -$$

$$-\frac{1}{2}C_3' D_{+}^{z}D_{-}^{z}\ (\underline{u}(0, n, i\text{-}1) + \underline{u}(1, n, i+1)) = 0$$

Right side (m = a)

$$D_{-}^{x}D_{0}^{t}\ \underline{u}(a, n, i) + \frac{1}{2}C_1' D_{+}^{t}D_{-}^{t}\ (\underline{u}(a, n, i) + \underline{u}(a\text{-}1, n, i)) +$$

$$+ \frac{1}{2}C_2^{T} D_{+}^{t}D_{0}^{z}\ (\underline{u}(a, n, i\text{-}1) + \underline{u}(a\text{-}1, n, i)) +$$

$$+ \frac{1}{2}C_3' D_{+}^{z}D_{-}^{z}\ (\underline{u}(a, n, i\text{-}1) + \underline{u}(a\text{-}1, n, i+1)) = 0 \qquad (3.8)$$

The three differential operators $D_{-}^{z}, D_{+}^{z}\ and\ D_{0}^{z}$ are backward, forward and central differential operators with respect to the variable z; i.e.

$$D_{+}^{z}u_{j,k}^{n} = (u_{j,k+1}^{n} - u_{j,k}^{n})/\Delta z$$

$$D_{0}^{z}u_{j,k}^{n} = (u_{j,k+1}^{n} - u_{j,k-1}^{n})/2\Delta z.$$

The matrices C_1' and C_3' which were introduced in [35] have the following form

$$C_1' = \begin{bmatrix} 1/v_p & 0 \\ 0 & 1/v_s \end{bmatrix}; \quad C_3' = \frac{1}{2}\begin{bmatrix} v_p - 2v_s & 0 \\ 0 & v_s - 2v_p \end{bmatrix}$$

and C_2^{T} is the transposed matrix of C_2.

For the corner points and for their first neighboring points on the boundaries, Clayton and Engquist suggested using rotated formulation of the approximation A1 from equation (3.5). The rotated A1 is for:

Bottom-right corner

$u_z + u_x + Mu_t = 0$

$$(D_-^z + D_-^x + M(v_p, v_s)D_-^t)u(m,n,i) = 0$$

where (m, n) = (a, a-1); (a-1, a); (a, a)

Bottom-left corner

$$(D_-^z - D_+^x + M(v_s v_p), D_-^t)u(m,n,i) = 0 \quad (3.9)$$

where (m, n) = (0, a-1); (1, a); (0, a) and the newly introduced matrix M is

$$\mathrm{M}(v_s v_p) = \frac{1}{\sqrt{2}}\begin{pmatrix} 1/v_s + 1/v_p & 1/v_s - 1/v_p \\ 1/v_s - 1/v_p & 1/v_s + 1/v_p \end{pmatrix}$$

3.2.3.2. Free surface

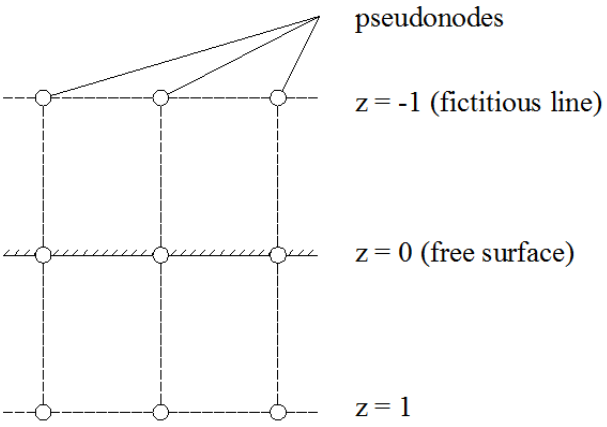

Figure 3.4 Pseudonodes at the free-surface boundary

For completing the model another boundary is left. The upper border, as mentioned previously is free surface. Because the points could not be solved only by the elastic wave equation, additionally new pseudonodes should be introduced. As it can be seen from figure 3, the free surface boundary has coordinate z = 0, and the pseudonodes will have index -1. The unknown displacement for these nodes will be calculated by the stress free conditions (3.3). The finite difference code for (3.3) is:

u(x, -1, t) = u(x, 0, t) + 0,5[w(x+1, 0, t) – w(x-1, 0, t)]

w(x, -1, t) = w(x, 0, t) + 0,5(1-γ^2)[u(x+1, 0, t) – u(x-1, 0, t)] (3.10)

Remark: equation (3.10) have this form only if grid size is dx = dz = h.

Finally, for the corner points where the intersection is between the vertical absorbing boundaries and the fictitious line first-order boundary conditions are used, according to [35], to determine their displacements. So, the schemes for these corner points are:

$(D_+^x - C_1' D_+^t)\underline{u}(0, -1, t) = 0$

$(D_-^x + C_1' D_+^t)\underline{u}(a, -1, t) = 0$ (3.11)

3.2.4. Source

The term which represents the source in the equation of motion inherits the following expression $\delta(r - r_0)f(t)$. One can easily recognize the Dirac-Delta function which has value infinity when r = r_0. That means that at the point where the force is applied, the stresses are going to infinity. To avoid this, I applied the source in four surrounding points with the same function in time (3.6) producing radial displacements equal in all directions.

3.2.5 Stability condition

3.2.5.1 Grid mesh

A physically meaningful calculations requires that the finite difference algorithm be stable, i.e., the difference between the exact and the numerical solutions of a finite difference equation must remain bounded as the time index i increases, Δt remaining fixed for all m and n [36]. The authors in [37] have shown that the system of equations (3.7) is stable provided that:

$$F = \frac{\alpha \Delta t}{h} \leq \left(1 + \frac{\alpha^2}{\beta^2}\right)^{-1/2} \quad (3.12)$$

for all α and β. Equation (3.12) can be also written in more revealing form

$$\Delta t \leq \frac{h}{(\alpha^2 + \beta^2)^{1/2}} \quad (3.13)$$

which shows that the time increment cannot be chosen arbitrary but rather must obey a constraint imposed by the choice of a grid interval h as well as the values of the P- and SV-wave velocities in particular homogeneous layer [30].

3.2.5.2 Absorbing boundaries

The stability of the absorbing boundaries is referred to the ratio of the SV- and P-wave velocities β/α. Experimenting with this ratio, the authors of [37] proved that the instability appears when the ratio is smaller than 0.46. The instability of the absorbing boundaries can be seen on the following figure 4 token from [37]:

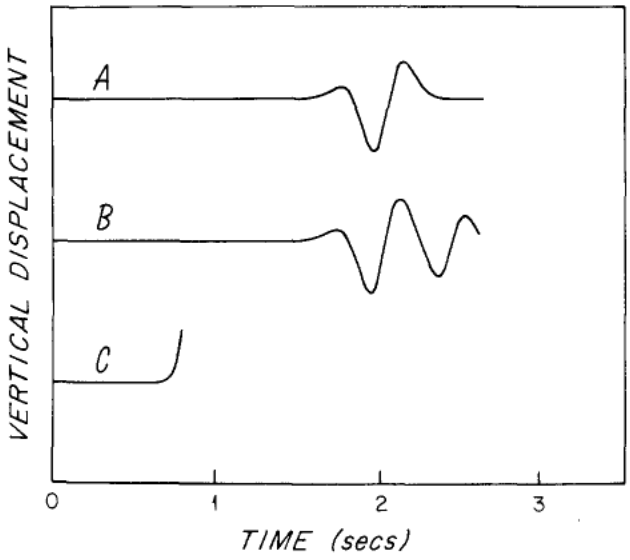

Figure 3.5 Instability of absorbing boundaries

To prove the instability, Emerman and Stephen built a model with 304x304 grid points with interior finite-difference scheme from [38] modified to rectangular coordinates. The source is defined as line source according to [30] with $t_s = 0.6$ and $\xi = 50$. In both directions they have same grid size $\Delta x = \Delta y = 0.01$km, the time step $\Delta t = 0.04375$s and velocities $v_p = 2.0$ km/s and $v_s = 0.5$km/s, with ground density $\rho = 1.3$ gm/cm^3. The three curves on figure 3.4 are: A-modified absorbing boundary by the authors; B-reflecting boundary; C-Absorbing boundary from [35]. Curve A is indistinguishable from the analytical solution for a whole-space, curve B is strongly contaminated by the reflection from the right boundary of the model and curve C clearly demonstrate the instability of the absorbing boundary with ration vs/ vp < 0.46 (in this experiment it is 0.25).

Beside the instability due to the ratio, according to some authors (e.g. [38], [39]) inappropriately defined free surface boundary conditions can derive a finite difference solution into instability when the velocity ratio is smaller than some critical value.

CHAPTER IV
RESULTS

4.1 Input parameters

In this chapter, the results obtained from four different models are shown. Three of the models are bounded with the Absorbing boundary conditions and stress-free boundary and one is bounded with boundaries with fixed displacements u = w = 0. First three models: Model 1, Model 2 and Model 3, have different ground characteristics representing three typical types of ground: mud (v_s=250m/s; v_p=250$\sqrt{3}$ m/s), clay (vs=400m/s; vp=400$\sqrt{3}$ m/s) and rock mass (vs=2500m/s; v_p=2500$\sqrt{3}$ m/s) respectively. The fourth model, Model4, has fixed boundaries and responds to the mud model with ABC's – Model 1. All of the models have same mesh size with 40 points in each direction, separated with equal spacing of 2m in both directions.

4.2 Results

If the mesh size is smaller than 5000x5000, the selection of programming software doesn't play big role, because the exactness by almost all programming languages in these margins doesn't vary. For this master work, the modules are written in Java's Eclipse. As an object-oriented language it contains classes which can be used for graphical and numerical representation of obtained results. The graphical output is colored in that way such that the red one represents the highest values and the dark blue is color for zero values. All other colors are representing in logical manner some values between the zero-values and the maximum.

Because the P-SV wave's problems are dealing with two unknown displacement in x- and z-direction, all results are representing the radial displacement at grid and boundary points in time. The radial displacement is calculated by the following equation:

$$r = \sqrt{u^2 + w^2} \tag{4.1}$$

where r is the radial displacement, u is the displacement in x-direction and w is the displacement in z-direction.

Due to the stability condition (3.13) different time step increments must be applied when the velocities in the models vary. Hence the graphical outputs are given by time in seconds. Time sections are different for the models and are chosen such that in the figures can be seen what is characteristic for the model.

In this chapter contains only graphical result illustration. Some of the written results are used further in the next chapter as interpretation of the results shown by the following figures.

4.2.1 Comparison between Model 1 and Model 4

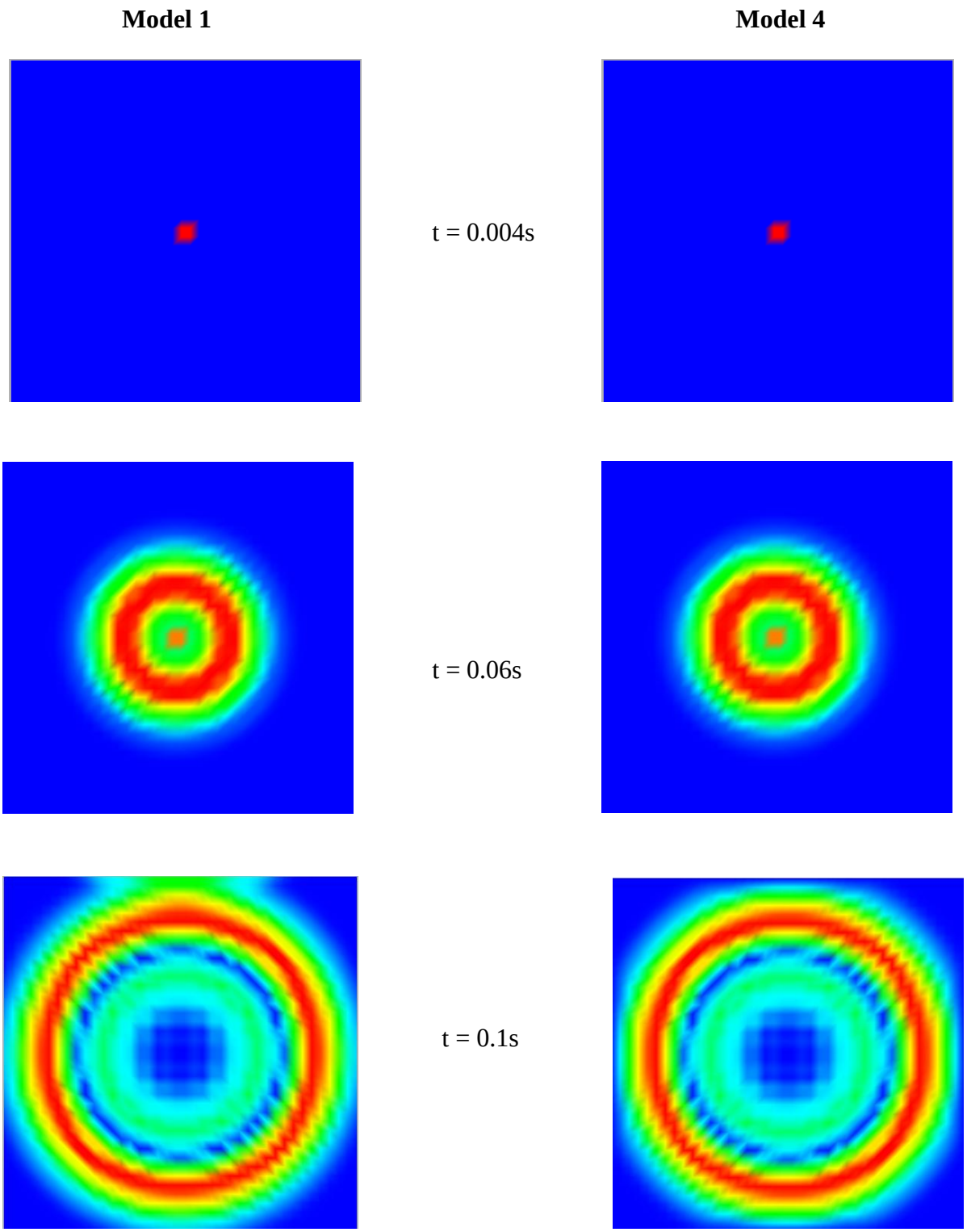

Figure 4.1 Radial displacement by the Model 1 and Model 4 at time t=0.004s; t=0.006s and t=0.1s

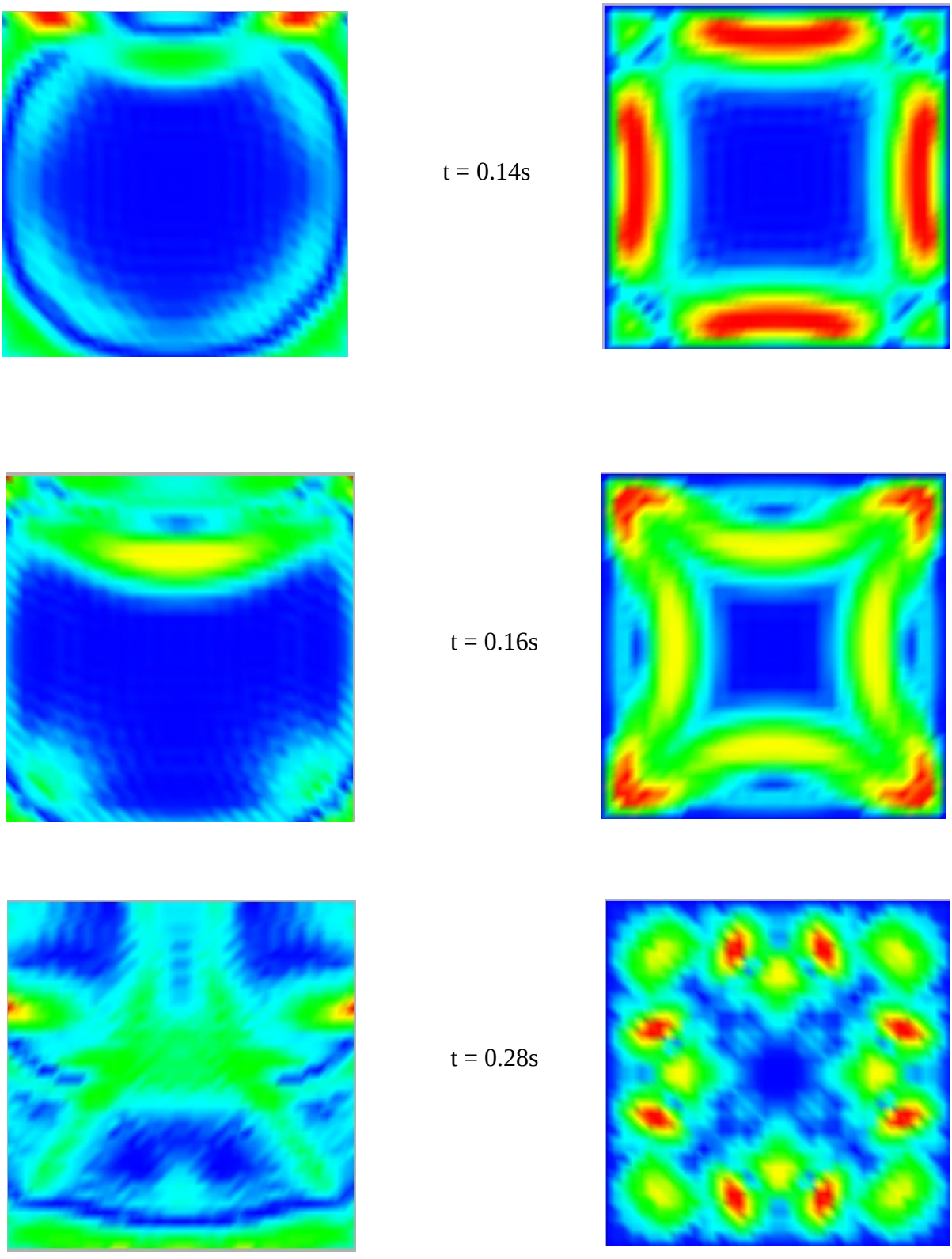

Figure 4.2 Radial displacement by the Model 1 and Model 4 at time t=0.14s; t=0.16s and t=0.28s

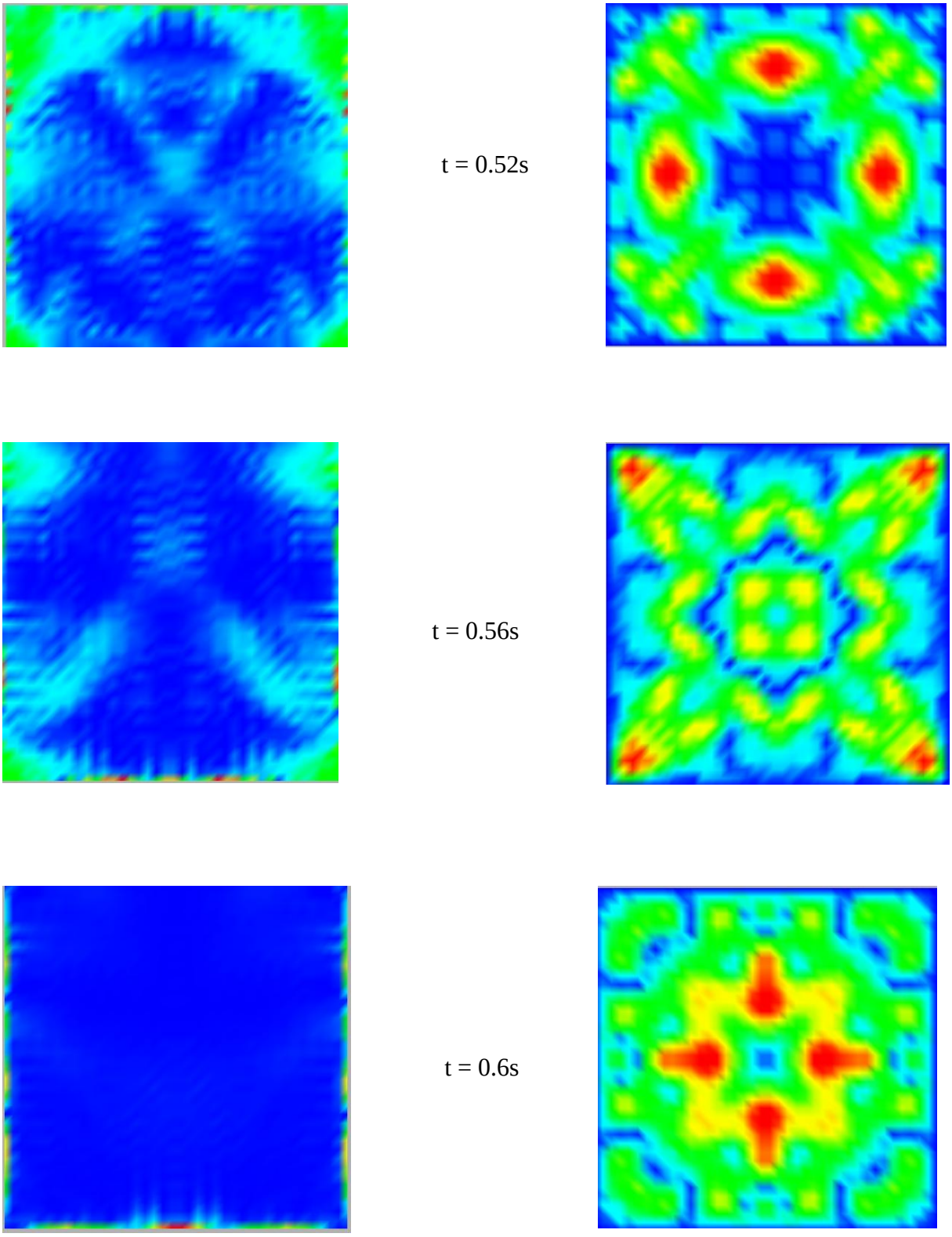

Figure 4.3 Radial displacement by the Model 1 and Model 4 at time t=0.52s; t=0.56s and t=0.60s

4.2.2 Model 2 and Model 3

Model 2 **Model 3**

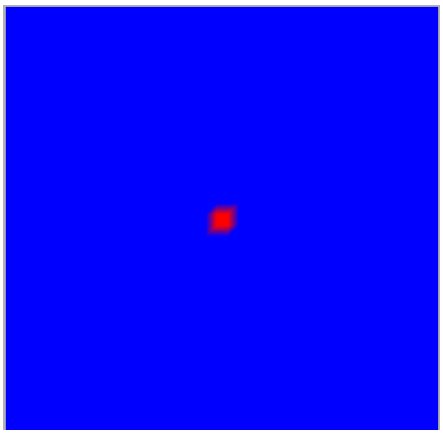

t = 0.002s

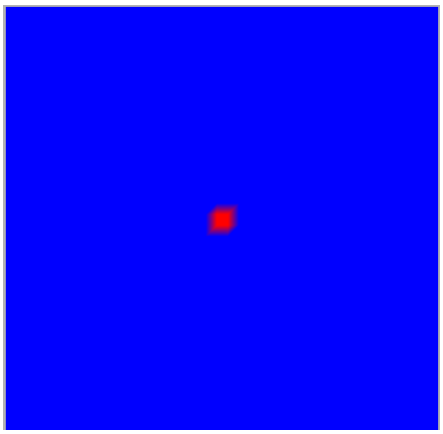

t = 0.0004s

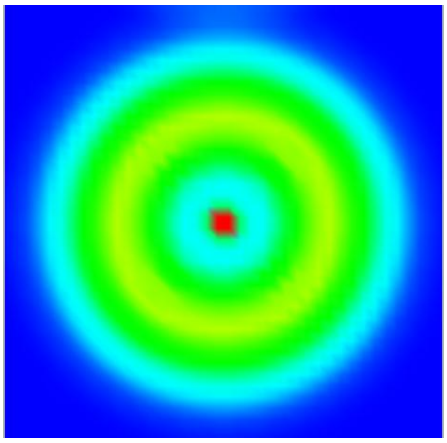

t = 0.06s

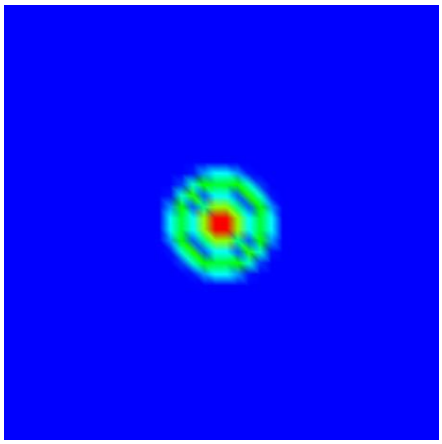

t = 0.002s

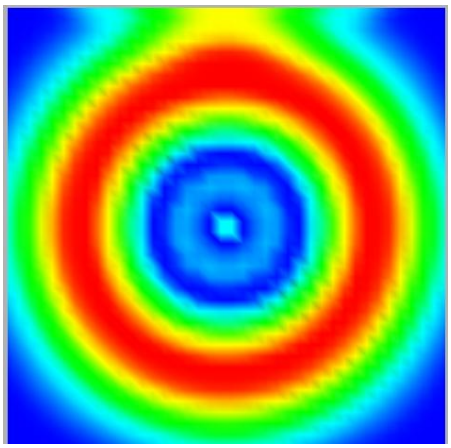

t = 0.07s

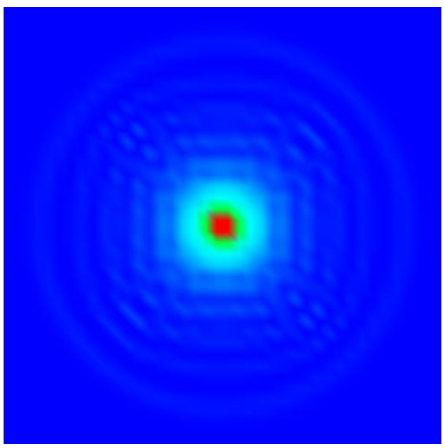

t = 0.008s

Figure 4.4 Radial displacement by the Model 2 at time t=0.004s; t=0.06s and t=0.07s and Model 3 at time t=0.004s; t=0.002s and t=0.008s

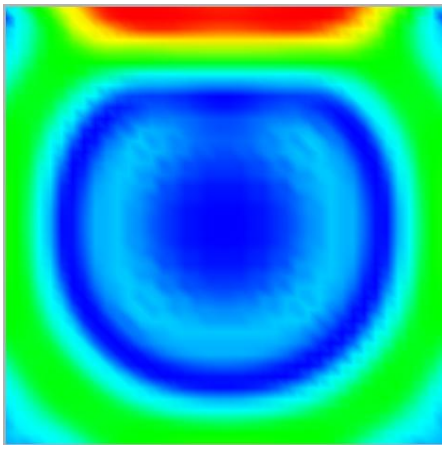

t = 0.08s

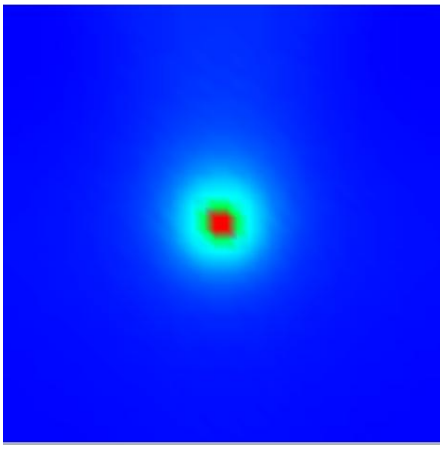

t = 0.036

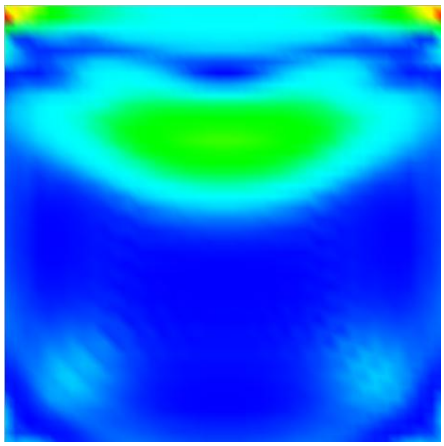

t = 0.12s

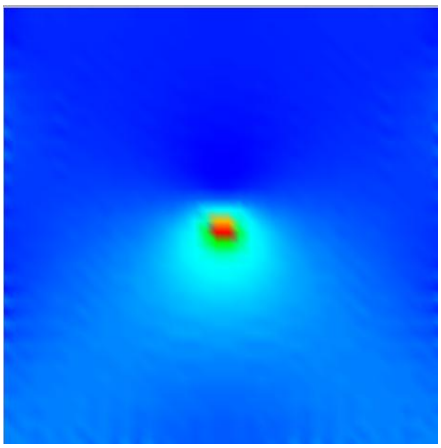

t = 0.056

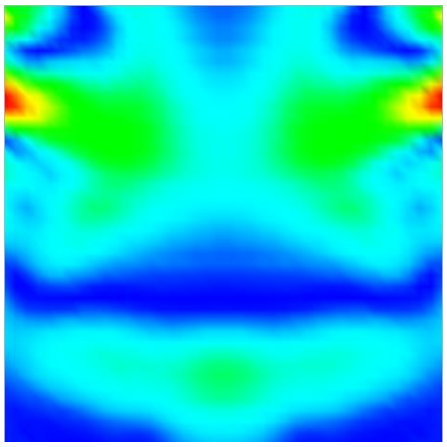

t = 0.18s

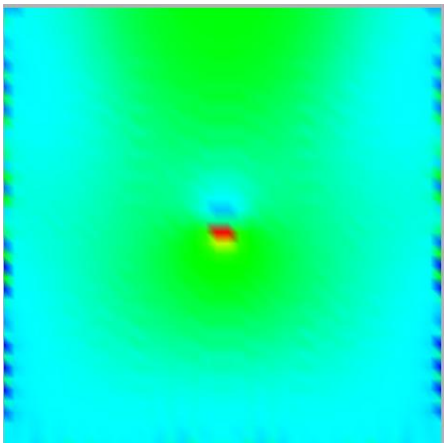

t = 0.064s

Figure 4.5 Radial displacement by the Model 2 at time t=0.08s; t=0.12s and t=0.18s and Model 3 at time t=0.036s; t=0.056s and t=0.064s

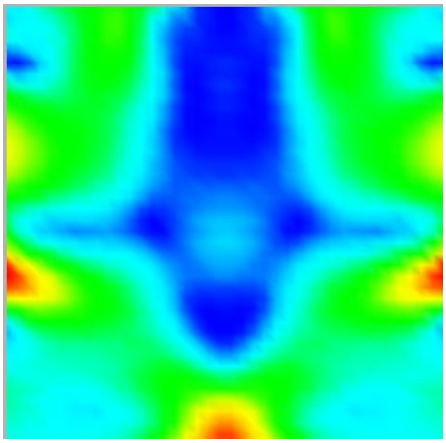

t = 0.28s

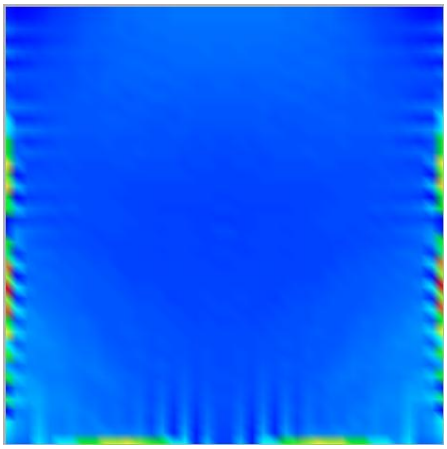

t = 0.08s

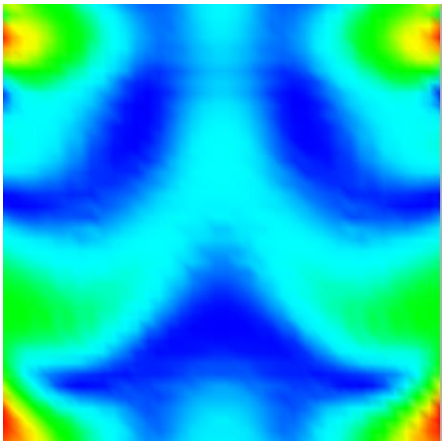

t = 0.36s

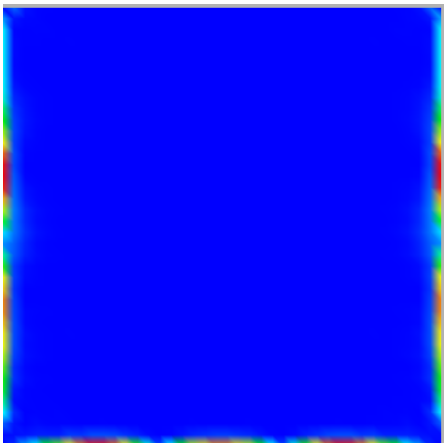

t = 0.1s

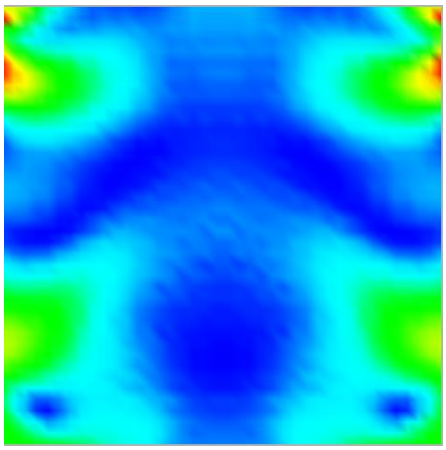

t = 0.37s

Figure 4.6 Radial displacement by the Model 2 at time t=0.28s; t=0.36s and t=0.37s and Model 3 at time t=0.08s and t=0.1s

CHAPTER V
INTERPRETATION OF RESULTS

5.1 Interpretation of results

The first row of the two panels on Figures 4.1 and Figure 4.4 are at time equal to the first time incremental. Mentioned previously in section (3.1.2) at time t=0s all displacements are equal to zero, and after the first time incremental only values of amplitude of the source function are applied at the four source points. The displacement at these source points and some of the neighboring points in Model 1 are:

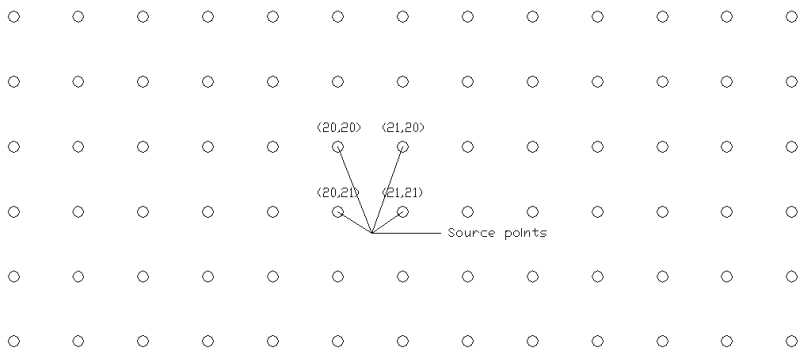


```
0.00000     0.00000     0.00000       0.00000     0.00000     0.00000
0.00000     0.00000     0.00000       0.00000     0.00000     0.00000
0.00000     0.00000   -2.31642E-01    2.31642E-01 0.00000     0.00000
0.00000     0.00000   -2.31642E-01    2.31642E-01 0.00000     0.00000
0.00000     0.00000     0.00000       0.00000     0.00000     0.00000
0.00000     0.00000     0.00000       0.00000     0.00000     0.00000
u-displacements at source points

0.00000     0.00000     0.00000       0.00000     0.00000     0.00000
0.00000     0.00000     0.00000       0.00000     0.00000     0.00000
0.00000     0.00000   -2.31642E-01  -2.31642E-01  0.00000     0.00000
0.00000     0.00000    2.31642E-01   2.31642E-01  0.00000     0.00000
0.00000     0.00000     0.00000       0.00000     0.00000     0.00000
0.00000     0.00000     0.00000       0.00000     0.00000     0.00000
w-displacements at source points

0.00000     0.00000     0.00000       0.00000     0.00000     0.00000
0.00000     0.00000     0.00000       0.00000     0.00000     0.00000
0.00000     0.00000   3.275913E-01    3.275913E-01 0.00000    0.00000
0.00000     0.00000   3.275913E-01    3.275913E-01 0.00000    0.00000
0.00000     0.00000     0.00000       0.00000     0.00000     0.00000
0.00000     0.00000     0.00000       0.00000     0.00000     0.00000
r-displacements at source points
```

Figure 5.1 u-, w- and r-displacements at the four source points of Model 1 at time t=0.004s

The u-displacements are chosen to induce positive displacements in right column and negative in the left column. The upper row of the w-displacements initiates negative displacements and the lower row positive. By using equation (4.1), equal radial displacements for all source points are obtained. As it can be seen, all neighboring points have still no displacements. Hence we have red square (see Figure 4.1 and Figure 4.4) only in the middle of the model and the rest is colored with dark blue. Because these source points

are satisfying the wave equation as well, they never achieve the maximum displacement which is given by the f(t) or f'(t) source functions.

The next row of figures in Figure 4.1 and Figure 4.4 are showing developed wave field which is moving towards the borders of the model. The wave fields have perfect circle form and there is simple explanation how can be obtained this form. The more grid points are used the better is the graphical output and the circle line. For the explanation of the circle-form wave field, I used the following displacements from Model 1 at the source and some neighboring points (see Figure 5.1):

```
0.0 0.0   0.0       0.0     0.0      0.0      0.0      0.0    0.0 0.0
0.0 0.0   0.0       0.0     0.0      0.0      0.0      0.0    0.0 0.0
0.0 0.0 -0.00361 -0.02533 -0.03619  0.03619  0.02533  0.00361 0.0 0.0
0.0 0.0 -0.03257 -0.11220  0.02171 -0.02171  0.11220  0.03257 0.0 0.0
0.0 0.0 -0.09410 -0.07962 -0.31663  0.31663  0.07962  0.09410 0.0 0.0
0.0 0.0 -0.09410 -0.07962 -0.31663  0.31663  0.07962  0.09410 0.0 0.0
0.0 0.0 -0.03257 -0.11220  0.02171 -0.02171  0.11220  0.03257 0.0 0.0
0.0 0.0 -0.00361 -0.02533 -0.03619  0.03619  0.02533  0.00361 0.0 0.0
0.0 0.0   0.0       0.0     0.0      0.0      0.0      0.0    0.0 0.0
0.0 0.0   0.0       0.0     0.0      0.0      0.0      0.0    0.0 0.0
u-displacemetns

0.0 0.0   0.0       0.0      0.0      0.0      0.0      0.0    0.0 0.0
0.0 0.0   0.0       0.0      0.0      0.0      0.0      0.0    0.0 0.0
0.0 0.0 -0.00361 -0.03257 -0.09410 -0.09410 -0.03257 -0.00361 0.0 0.0
0.0 0.0 -0.02533 -0.11220 -0.07962 -0.07962 -0.11220 -0.02533 0.0 0.0
0.0 0.0 -0.03619  0.02171 -0.31663 -0.31663  0.02171 -0.03619 0.0 0.0
0.0 0.0  0.03619 -0.02171  0.31663  0.31663 -0.02171  0.03619 0.0 0.0
0.0 0.0  0.02533  0.11220  0.07962  0.07962  0.11220  0.02533 0.0 0.0
0.0 0.0  0.00361  0.03257  0.09410  0.09410  0.03257  0.00361 0.0 0.0
0.0 0.0    0.0      0.0      0.0      0.0      0.0      0.0   0.0 0.0
0.0 0.0    0.0      0.0      0.0      0.0      0.0      0.0   0.0 0.0
w-displacemetns

0.0 0.0    0.0    0.0        0.0      0.0      0.0      0.0   0.0 0.0
0.0 0.0    0.0    0.0        0.0      0.0      0.0      0.0   0.0 0.0
0.0 0.0 0.005118 0.041267 0.100825 0.100825 0.04126  0.005118 0.0 0.0
0.0 0.0 0.041267 0.158677 0.082535 0.082535 0.158677 0.041267 0.0 0.0
0.0 0.0 0.100825 0.082535 0.447795 0.447795 0.082535 0.100825 0.0 0.0
0.0 0.0 0.100825 0.082535 0.447795 0.447795 0.082535 0.100825 0.0 0.0
0.0 0.0 0.041267 0.158677 0.082535 0.082535 0.158677 0.041267 0.0 0.0
0.0 0.0 0.005118 0.041267 0.100825 0.100825 0.04126  0.005118 0.0 0.0
0.0 0.0    0.0      0.0        0.0      0.0      0.0      0.0   0.0 0.0
0.0 0.0    0.0      0.0        0.0      0.0      0.0      0.0   0.0 0.0
r-displacement
```

Figure 5.2 u-, w- and r-displacements at the four source points of Model 1 at time t=0.012s

Analyzing Figure 5.2 clearly can be seen that the u-displacements on the left half of the non-zero values (first three columns) have negative sign, which means that they are oriented opposite to the positive x-axis, which is the direction of the wave field left from the source. Opposite to that, values on the right half (last three columns) have positive signs and are corresponding to the direction of the wave filed right from the source. The same can be concluded for the w-values as well. Namely, values above the source (first three rows) have negative sign and values below the source have positive signs which correlate to the direction of moving of the wave field above and below the source.

For the perfect circle-form one must have symmetry about all axes. U- and w-displacements analyzed separately have symmetry only about x- and z-axis, respectively. But if one analyze the values of u- and w-displacements it can be recognized that the u-

displacements are having the same values as w-displacements but rotated about the source for 90 degrees. So by calculating the radial displacements for two points about spatial symmetry (the source is defined in four points, hence only vertical, horizontal and both diagonal symmetry can be analyzed) same values will be used and the difference in signs will be eliminated by giving them power of two. At the end the full symmetry can be seen in the r-displacements.

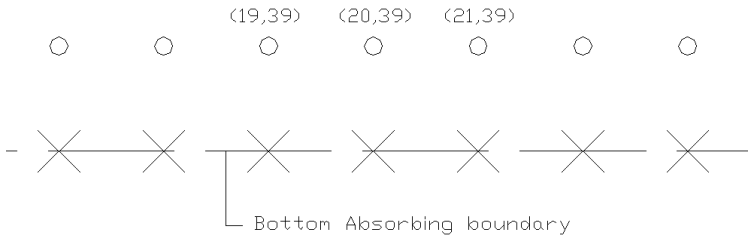

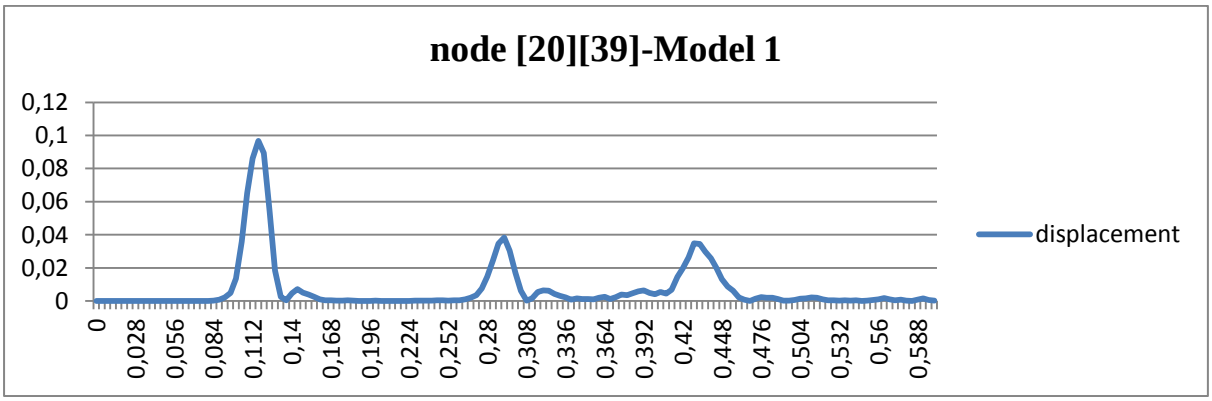

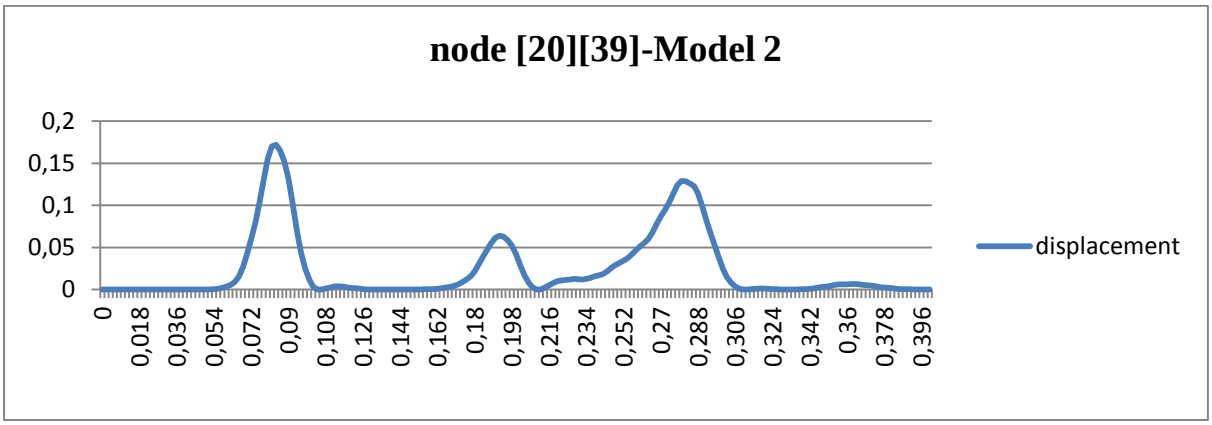

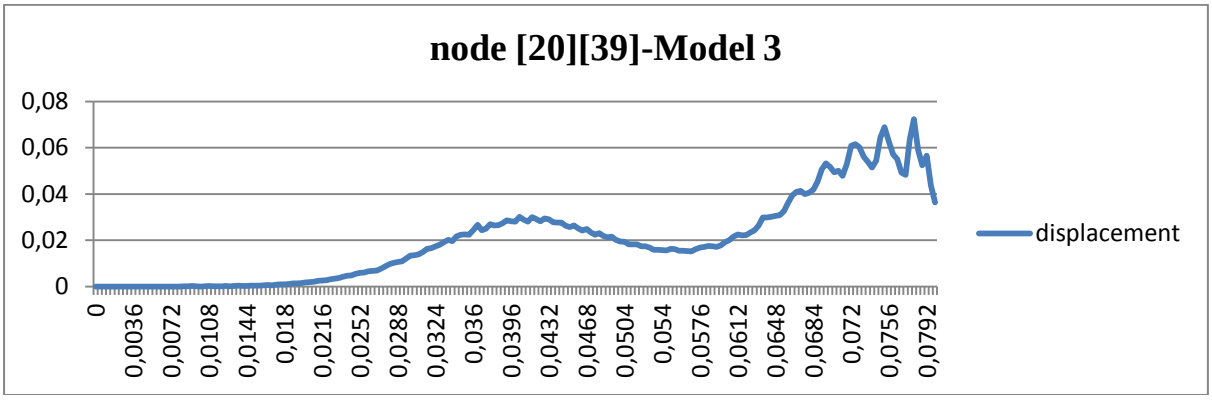

Figure 5.3 Displacement in time at node "node [20][39]" for Model 1, Model 2 and Model 3

The time needed to be formed the wave field is directly depended on the velocities of the waves. Also the time when the wave field is "hitting" the Absorbing boundaries and the free surface is related to the velocities of the waves. It can be simply calculated by the Newton equation $t=\frac{L}{v_p}$, where L is the distance from the source to the borders and v_p is the compressional velocity. If the wave field is formed continuously in time, the time needful the wave field to be formed should be added. For this characteristic of the wave fields I made the third row of figures in Figure 4.1 and Figure 4.4. The wave fields from Model 1 and Model 4 are having same velocities and hence the wave fields are approaching the borders at same time. Model 2 needs much shorter time compared to Model 1 and Model 3 loose the stability before the wave field is formed, which will be explained later. More clearly that can be seen in the Figure 5.3 where the displacements are measured at point with coordinate (20,39) which is the last point before the bottom absorbing boundary. This will be discussed again at the end of this chapter.

Figure 5.3 shows another characteristic that must be expressed when one deals with wave propagation. The displacements at this analyzed node are not the same. As mentioned previously the velocities are function of Lame parameters and density. When these parameters are changed indirectly the dumping ratio is changed as well.

The first two rows of figures in Figure 4.2 and Figure 4.5 are showing the different effect by different type of boundary conditions. In Model 4 where the displacements are prescribed (Dirichlet boundary conditions u=w=0) the waves can't go through the borders of the truncated model and they are reflected inside the computational region. That means that the energy is occupied between the borders and can't be dispersed outside the model with the moving wave field. This of course leads to wrong, unreal results. The reflection can be seen on the following figure as well, where the source point displacement is shown in time.

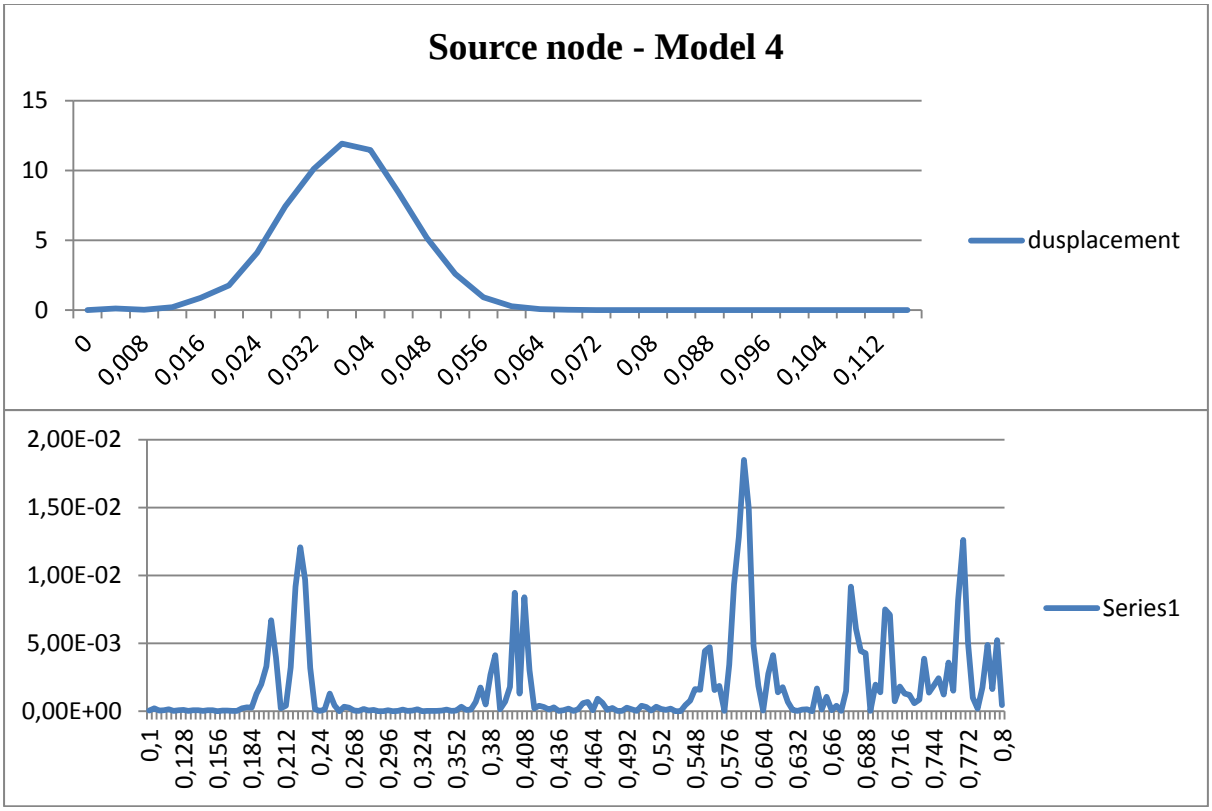

Figure 5.4 r-displacement in time at one of the four source nodes by Model 4

The top panel of Figure 5.4 shows already mentioned excitation due to the explosive source. The first disturbing in the lower panel is due to the wave fields which are reflected from the boundaries. The vibrations at higher time steps are showing that the energy is not disappeared and is closed inside the model.

In the figures from the previous chapter one can see that also in the Model 1 to Model 3 there is reflection from the top boundary. In these models the top boundary is representing the free surface. The free surface boundaries are Neumann boundary conditions, so these four models are confirming that the Dirichlet and Neumann boundary conditions are producing reflections. Opposite to this, the Absorbing boundary conditions fulfilled their function by letting the wave fields passing through them. Since they are approximation of the wave equation and there is interaction in two directions in the numerical model between the borders and the grid, they must maintain the symmetry which is coming from the wave field (about all axes) and lest the model would not lose its symmetry. The following figure is showing the displacements at the bottom-right and bottom-left corners of Model 1 and the symmetry can be recognized.

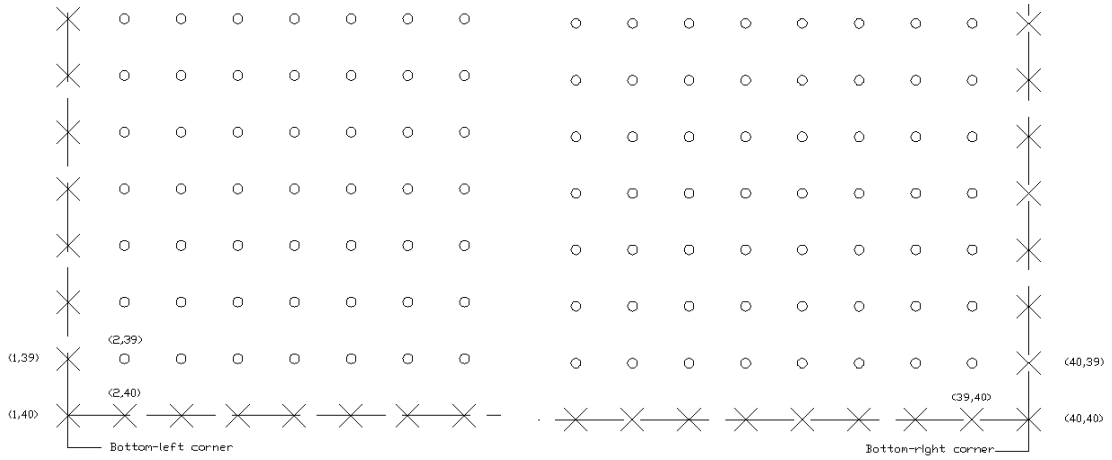

0.0581	0.0803	0.0834	0.1159	0.1029	0.0910	0.0752	0.0743
0.0273	0.0687	0.1058	0.1149	0.1206	0.1208	0.9103	0.0752
0.0214	0.0428	0.0820	0.1453	0.1297	0.1156	0.1208	0.0910
0.0970	0.0165	0.0718	0.0965	0.1589	0.1297	0.1206	0.1029
0.1502	0.0733	0.0490	0.0883	0.0965	0.1453	0.1149	0.1159
0.2104	0.1167	0.0386	0.0490	0.0718	0.0820	0.1058	0.0834
0.1906	0.1380	0.1167	0.0733	0.0165	0.0428	0.0687	0.0803
0.2038	0.1906	0.2104	0.1502	0.0970	0.0214	0.0273	0.0581

Bottom-left corner

0.0743	0.0752	0.0910	0.1029	0.1159	0.0834	0.0803	0.0581
0.0752	0.9103	0.1208	0.1206	0.1149	0.1058	0.0687	0.0273
0.0910	0.1208	0.1156	0.1297	0.1453	0.0820	0.0428	0.0214
0.1029	0.1206	0.1297	0.1589	0.0965	0.0718	0.0165	0.0970
0.1159	0.1149	0.1453	0.0965	0.0883	0.0490	0.0733	0.1502
0.0834	0.1058	0.0820	0.0718	0.0490	0.0386	0.1167	0.2104
0.0803	0.0687	0.0428	0.0165	0.0733	0.1167	0.1380	0.1906
0.0581	0.0273	0.0214	0.0970	0.1502	0.2104	0.1906	0.2038

Bottom-right corner

Figure 5.5 r-displacements at bottom right and bottom-left corners

The bottom boundary is defined by the paraxial approximation A2 (see eq.3.5) and this definition is valid starting from point (3,40) up to (28,40). For the rest of the points, two points at the beginning and end of the row representing the corners, the approximation A1 is

used. By comparing the r-displacements at the corners, one can see that the symmetry is not disturbed.

Although the absorbing boundaries make absorption of energy, they are defined as approximations and thus they must produce some reflection. The reflection is dependent on the order of the paraxial approximation and the angle of incidence. The higher is the order of the paraxial approximation the higher is the exactness. For the dependence on the incident angle the authors of [22] have given the following results:

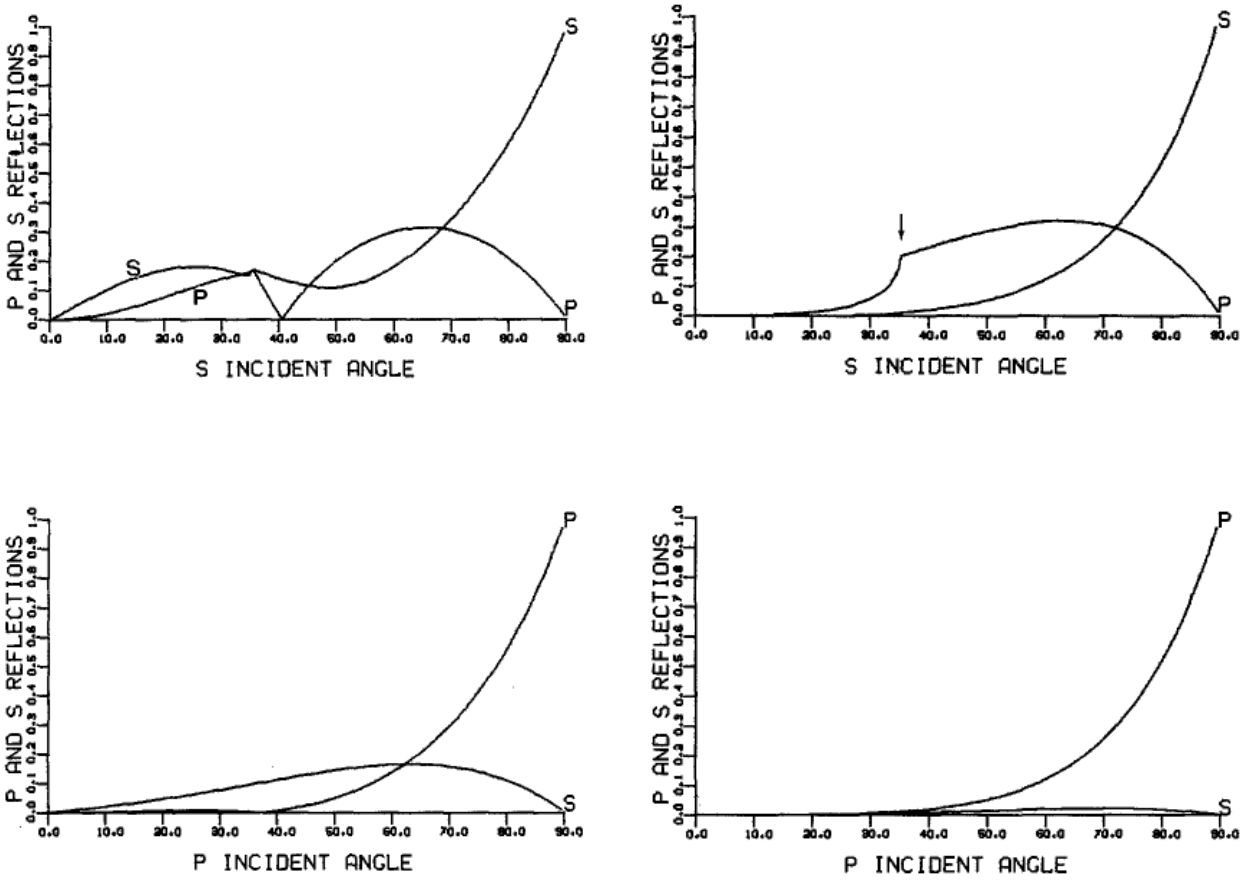

Figure 5.6.Reflection coefficient for A1 (left panel) and A2 (right panel) for incident S-waves (upper graphics) and incident P-waves (lower graphics)

To find the effective reflection coefficients for elastic eaves in the authors in [22] assumed that wave potentials have solution of form:

$$\Phi = \Phi_0 \exp i\left(\frac{\omega}{\alpha}\right)(l_\alpha x + n_\alpha z) + r_p \exp i\left(\frac{\omega}{\alpha}\right)(l_\alpha x - n_\alpha z)$$

$$\Psi = \Psi_0 \exp i\left(\frac{\omega}{\beta}\right)(l_\beta x + n_\beta z) + r_s \exp i\left(\frac{\omega}{\beta}\right)(l_\beta x - n_\beta z)$$

where $l_\alpha, n_\alpha, l_\beta \; and \; n_\beta$ are the direction cosines of the wave front. For incident compressional waves, $\Phi_0 = 1$ and $\Psi_0 = 0$ and for incident shear waves it is opposite. The displacement fields can be found by transformation

$$u = \Phi_x + \Psi_z$$

$$w = \Phi_z - \Psi_x$$

The displacements are substituted in the equation (3.5) and the reflection coefficient r_p and r_s are obtained.

Figure 5.6 clearly shows that the reflections are much smaller by the A2 approximations than by A1 approximations. It should be noted that angles where the reflection coefficient is large, correspond to waves traveling almost parallel to the boundary [22]. But it is logical to expect that this wave would strike another boundary and not that one which is parallel to their direction.

The difference in the reflections can be seen in the first and second row of figures in Figure 4.2 and 4.5. The first row is when the wave field is passing through the border where A2 is applied and the second row is showing the wave field passing through corners where A1 is applied. It means that in the first case we have incident angle equal to zero and in second case wave approaching the corners with incident angle around 45^0. A1 are causing reflections that are even visible. Confirmation about this is shown on the next figure:

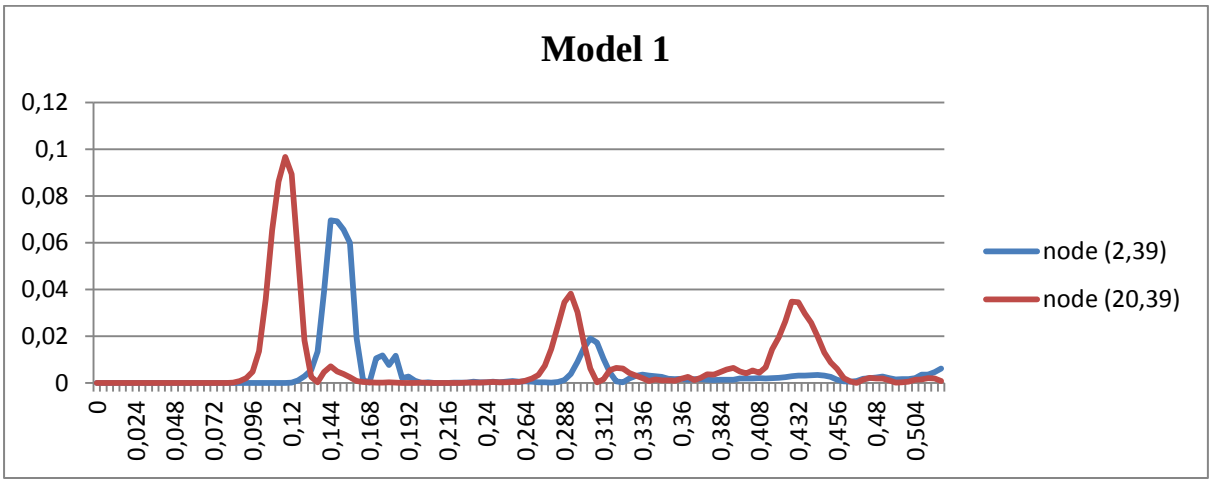

Figure 5.7 r-displacements in time for nodes (2,39) and (20,39) from Model 1

On the graph are shown the displacements in time for node (2,39) as neighbor point to absorbing boundary defined by A1 and node (20,39) as point next to the boundary where A2 paraxial approximation is used. The peaks which are next to the wave field peak are result of the reflections and grid dispersion (will be discussed at the end of the chapter). The following peak at node (2,39) (the blue line) is much bigger than the same peak at node (20,39) (red line) which confirms that the order of the paraxial approximations and the angle of incidence makes A1 approximation induce greater reflections than A2. The reflection coefficient in Model 1 is in the margins of 5-10%.

Beside the reflections, on Figure 5.7 one can see that because the difference in distances between the source and bottom boundary is shorter than the distance between the source and the corners, the peaks are not happening at the same time. Since the distance from the source to the node (20,39) is shorter the displacements are first developed at the this node. Also the effect of the dumping can be recognized by the values of the peaks.

The biggest disadvantage of these boundary conditions is the corners. Clayton and Engquist [22] tried to improve that by introducing the A1 approximation at the corners. But this is only valid when two absorbing boundaries are intersecting. In the top-left and the top-right corners the intersection is between the free surface and the absorbing boundary and thus A1 is not an option. These corners are uncovering the greatest weakness of the model. They produce instability which have influence at the rest points. Namely, calling back Figure 5.6 one can see that the displacements for node (20,39) have three peaks. The first one is from the wave field coming from the source (firs row on the left panel of Figure 4.2 and Figure 4.5); the second one is from the wave field which is reflected from the free surface (third row of left panel on Figures 4.2 and 4.5) and the last one is result of the instability at the top-left

and top-right corners. On the second row of figures on Figure 4.2 and 4.5 there are extremes colored with red exactly at those corners. In the next row one can see that these extreme values are moving downwards and in the first row of figures in Figure 4.6 can be seen that these extremes produced at the top corners influence the displacements on the bottom boundary as well. As shown on the last two rows on figures on Figure 4.6 these extremes are leaving the model but meanwhile new one are produced.

On the last two rows on Figure 4.4 another disadvantage of the Absorbing boundaries is illustrated. These boundary conditions are losing the stability after some number of time steps by permanent increment of the displacements. The displacement in time for node (20,40) on the bottom-boundary would look like the following figure:

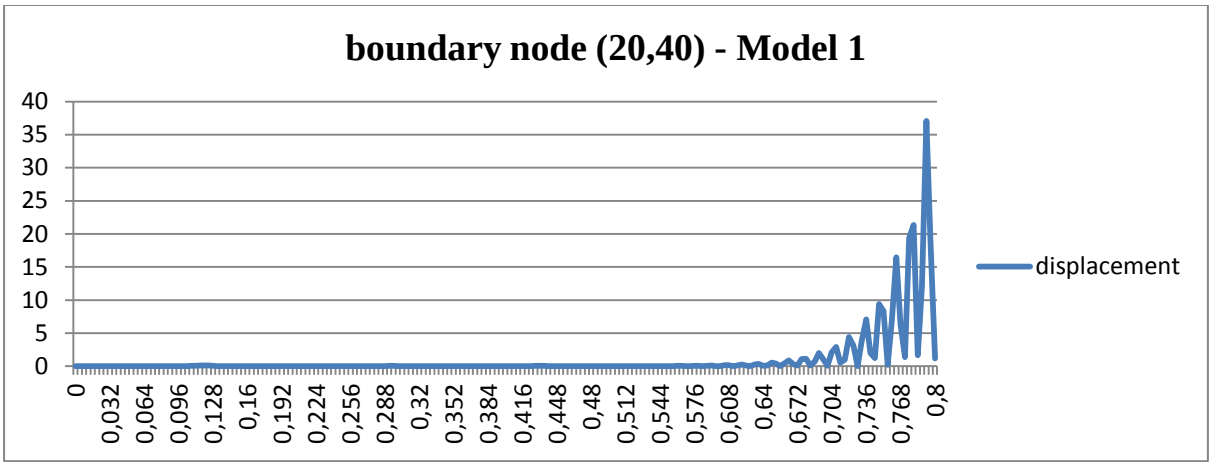

Figure 5.8 Instability of Absorbing boundaries in time

This would be no problem if the instability is happening only on the boundaries. But because of the interaction between the grid mesh and the absorbing boundaries, the increment is transferred in the inner part of the model.

Most of the previous interpretation was referred to the Model 1, Model 2 and Model 4. The results for Model 3 shown on the right panel on the Figure 4.4 to Figure 4.6 are not satisfying. It is not a weakness of the boundaries, but because the wavelength is proportional to the wave velocity and hence the model doesn't capture the full wavelength and that is not allowed. So increasing the velocity means that it is needed the model to be increased as well. The dimensions of the model must be careful defined such that the model would represent the full wave field and it's propagation through the medium.

Another important issue which should be stressed out is the distance between the grid points. This problem was analyzed by Boore [40] and Alford et al. [41]. Grid dispersion produce a "normal" variation of velocity with frequency, that is, the higher signal frequencies are delayed relative to the lower signal frequency and substantial "tailing" of the signal arises. When wave propagates in discrete grid it is progressively dispersed with increasing the travel time. This dispersions increase in prominence as the grid interval h becomes larger [30]. As a rule of a thumb, the number of grid points per wavelength at the upper half-power frequency of the source should be approximately ten or more in order to satisfy limit grid dispersion [41]. From the four models Model 1 and Model 4 have less than 10 points per wavelength while Model 2 and Model 3 are satisfying the criteria of minimum points per wavelength. The stronger grid dispersion can be seen in Figure 5.3. On the panel for the Model 1 the maximal radial displacements are smaller than those from the Model 2.

For illustration of the grid dispersion the following picture is used:

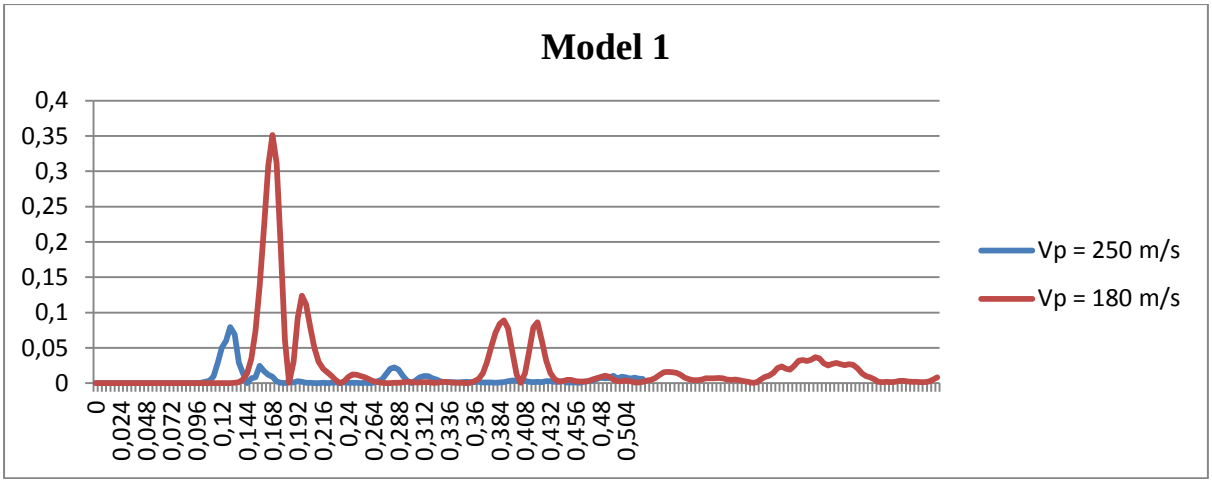

Figure 5.9 Grid dispersion for different velocities

By decreasing the velocity, the wavelength is decreased too. So, for same grid mesh less grid points are used per wavelength and hence the grid dispersion ("tailing" peak) is bigger.

Another characteristic is obvious on this figure. For that purpose the following relations of parameters should be analyzed:

$v_p \downarrow \rightarrow \ \rho \uparrow \rightarrow e \ \downarrow \rightarrow G \uparrow \rightarrow \ \gamma \downarrow \rightarrow D \downarrow$

If one decrease the wave field velocity v, the density ρ must be increased, thus the pore coefficient e is smaller and therefore the shear moduli G have increment. Higher shear moduli gives smaller shear strain amplitude γ and this leads to smaller dumping coefficient D. So, for smaller velocities the dumping is smaller too and that give higher displacements, what actually is shown on the last figure.

CHAPTER VI
CONCLUSIONS

6.1. Conclusions

The model developed in this theses is another confirmation that the Dirichlet boundary conditions (fixed displacements) and the Neumann boundaries (stress free boundary) are boundary conditions which produce reflection. Due to the reflection, the whole incoming energy coming towards the boundary with the wave field is reflected back in the model and hence the energy is captivated inside the model. The model with this kind of boundaries cannot provide accurate results. Before the artificial boundaries were introduced, the researchers used very large models to avoid the effect of the reflections in some lower time steps. The bigger the model is build, the more computational time and the complexity of the problem is increased. That time that was big problem because the computers didn't have the performance of nowadays machines. This is the background of the idea to invent the artificial boundary conditions.

Despite that more than 30 years are gone since the Absorbing boundary conditions were introduced by Clayton and Engquist, these boundaries are often used in the practical and research applications nowadays. They are simple to apply, in the problem of wave propagation and artificial boundary conditions. They don't require long computational time and hence are very computationally inexpensive. Now in the era of fast computers this is secondary problem, and the main priority is to get more accurate results. A good boundary condition nowadays is definition for boundary where the reflected energy is less than 2% of the income energy. The Absorbing boundaries used in presented model were based on paraxial approximations of first and second order. The used paraxial approximations don't satisfy the modern definition of accurate boundary condition at the corners and higher angle of incidence. On the rest of the boundary the reflection is much lower. The accuracy of the numerical solution can be improved by increasing the order of the approximation.

The proposed model showed some weaknesses when the absorbing boundaries should be combined with the stress-free boundary. The problem arises in the corners of intersection between the line with pseudonodes, needed for the calculation of the free surface, and the vertical absorbing boundaries. The difficulty is because the first order approximation used for the other corners, where the intersection is between two absorbing boundaries, is not valid for these corners. What remains is pure 90^0 edge which by many authors is called as "threat" to the numerical stability of the model. With this model it was confirmed the numerical inexactness of the corners with first order paraxial approximations. The generated reflection is greater than 5%. At the intersection between absorbing boundary and pseudonodes numerical instability is occurred. It has further effects on the displacement of the bottom boundary.

With the developed model it is confirmed that the numerical stability of the absorbing boundaries is dependent on the ratio of the shear and compressional velocities. The lower limit for this ratio is 0.46.

The correct results are dependent on the correctly set gird mesh. At the end of Chapter V is stressed out that the distances between the points of the grid should be chosen such that there are at least 10 points per wavelength. Also inexact results can occur if the dimensions of the model are not proportional to the wavelength.

6.2. Possibilities and ideas for further upgrade to the Model

In the past 30 years many researches are done and a lot of improvements are suggested. This work is review of the Absorbing boundary conditions [22]. It can be further developed in model of some of the proposed improvements and can be made comparison of the obtained results from different boundary conditions. The model can be adapted for practical purpose as well. With this formulation only one type of ground is available. There is possibility to introduce an interface between two layers with different ground properties, which can help to obtain more real model representing truncation of i.e. underground basis of analyzed object. Another step towards obtaining more real model is introducing the non-linearity of the ground, which, as mentioned previously, is one of the advantages of finite-difference numerical simulations. Of course in this format it has function of solver, for real practical usage one must add friendly user interface and very good output of the results.

REFERENCES

[1] Symeon V. Tsynkov, *Numerical Solution of the Problems on Unbounded Domains. A Review*, (1998)

[2] V. Gicev, *Investigation of Foundation-Structure Interaction for Incident Plane SH Waves*, PhD Dissertation at Univ. of South. California, (2005);

[3] B.Ehgquist and A. Majda, *Absorbing boundary conditions for the Numerical Solution of Waves*, Math. Comput. 31, (1977), pp 629-651;

[4] B.Ehgquist and A. Majda, *Radiation Boundary Conditions for Acoustic and Elastic Wave Calculations*, Commun. Pure Appl. Math. 32, (1979), pp 313-357;

[5] B.Gustafsson, *Far-Field Boundary Conditions for Time-Dependent Hyperbolic Systems*, SIAM J. Sci. Statist. Comput. 9, (1988), pp 812-828;

[6] L. Halpern, *Artificial Boundary Conditions for Incompletely Parabolic Perturbations of Hyperbolic Systems*, SIAM J. Math. Anal. 22, (1991), pp 1256-1283;

[7] I.L Sofronov, *Artificial Boundary Conditions which are Adequate to the Wave Equation Outside the Sphere*, Keldysh Inst. Appl. Math. Russian Acad. Sci., Preprint No. 42, (1992);

[8] I.L Sofronov, *Conditions of Complete Transparency on the Sphere for the Three-Dimensional Wave Equation*, Russian Acad. Sci. Dokl. Math. 46, (1993), pp 397-401;

[9] I.L Sofronov, *Generation of 2D and 3D Artificial Boundary Conditions Transparent for Waves Outgoing to Infinity*, Math. Institute A, Stuttgart University, Preprint No. 96 – 09, (1996);

[10] D. Givoli and J. B. Keller, *A Finite Elelment Method for Large Domains*, Comp. Meth. Appl. Mech. Engrg. 76, (1989), pp 41-66;

[11] J. B. Keller and D. Givoli, *Exact Non-Reflecting Boundary Conditions*, J. Comp. Phys. 82, (1989), pp 172-192;

[12] D. Givoli, *A Spatially exact Non-Reflecting Boundary Conditions for Time Dependent problems*, Comp. Meth. Appl. Mech. Engrg 95, (1992), pp 97-113;

[13] M. J. Grote and J. B. Keller, *Exact Non-Reflecting Boundary Conditions for Time-Dependent Wave Equation*, SIAM J. Appl. Math. 55, (1995), pp280-297;

[14] M. J. Grote and J. B. Keller, *Non-Reflecting Boundary Conditions for Time-Dependent Scattering*, J. Comp. Phys. 127, (1996), pp 52-65;

[15] I. Harari and T. J. R. Hughes, Analysis *of Computational Formulations Underlying in the Computation of Time-Harmonic Acoustics in Exterior Domains*, Comp. Meth. Appl. Mech. Ergr. 97, (1992), pp 103-124;

[16] M. J. Grote and J. B. Keller, *On Nonreflecting Boundary Conditions*, J. Comp. Phys. 122, (1995), pp 231-243;

[17] T. Hagstrom, S. I. Hariharan and D. Thompson, *High-Order Radiation Boundary Conditions for the Convective Wave Equation in Exterior Domains*, SIAM J. Sci. Comp. 25 (3), (2003), pp 1088-1101;

[18] G. K. Gachter and M. J Grote, *Dirichlet-to-Neumann Map for Three-Dimensional Elastic Waves*, Wave Motion 37 (3), (2003), pp 293-311;

[19] M. Premov and I. Spacapan, *Solving Exterior Problems of Wave Propagation Based on an Iterative Variation of Local DtN Operators*, Appl. Math. Model. 28 (3), (2004), pp 291-304

[20] J. Lysmer and R. L. Kuhlenmeyer, *Finite Dynamic Model for Infinite Media*, J. Eng. Mech. Div., (1969), pp 859-877;

[21] T. M. Hagstrom, *On the Convergence of Local Approximations of Pseudodifferential Operators with Applications*, NASA Technical Memorandum No. 106792, ICOMP-94-29, Lewis Research Center, November (1994);

[22] R. Clayton and B. Engquist, *Absorbing Boundary Conditions for Acoustic and Elastic Waves*, BSSA Vol.67, No.6, (1977), pp 1529-1549;

[23] R. L. Higdon, *Absorbing Boundary Conditions for Different Approximations to the Multidimensional Wave Equation*, Math. Comp. 47, (1986), pp 437-459;

[24] A. Bayliss and E. Turkel, *Radiation Boundary Conditions for Wave-Like Equations*, Commun. Pure Apll. Math. 33, (1980), pp 707-725;

[25] A. Bayliss and E. Turkel, *Far-Field Boundary Conditions for Compressible Flow*, J. Comp. Phys. 48, (1982), pp 182-199;

[26] D. Givoli and J. B. Keller, *Non-Reflecting Boundary Conditions for ElasticWaves*, Wave Motion 12, (1990), pp 261-279;

[27] D. Givoli and I. Patlashenko, *Optimal Local Non-Reflecting Boundary Conditions*,J. Appl. Num. Math. 27, (1998), pp 367-384;

[28] D. Givoli, *High-Order Nonreflecting Boundary Conditionswithout High-Order Derivatives*, J. Comp. Phys. 170, (2001), pp 849-870;

[29] S. Lee and L. F. Kallivokas, *Local Absorbing Boundaries of Elliptical Shape for Scalar Wave Propagation in a Half-Plane*, Fin. Elem. in Anal. and Design, (2004), pp 2063-2084;

[30] K. R. Kelly, R. W. Ward, S. Treitel and M. Alford, *Synthetic Seismogram: a finite difference approach*, Geophysics 41, pp 2-27;

[31] F. C. Karal and J. B. Keller, *Elastic wave propagation in homogeneous and inhomogeneous media*,J. Acoust. Soc. Am. 31, (1959), pp 694-705;

[32] J. Viieux, *P-SV wave propagation in heterogeneous media: Velocity-stress finite-difference method*, Geophysics 51, (1986), pp 889-901;

[33] F. S. Grant and F. G. West, *Interpretation theory in applied geophysics*, McGraw-Hill Book Co., Inc., (1965);

[34] M. Ottaviani, *Elastic Wave Propagation in two evenly-welded quarter-spaces,* BSSA 61, (1971), pp 1119-1152;

[35] M. Fuyuki and Y. Matsumoto, *Finite Difference Analysis of Rayleigh Wave Scattering at a Trench*, BSSA 70, (1980), pp 2051-2069;

[36] A. R. Mitchel, *Computational Methods in Partial Differential Equations*, New York, John Wiley&Sons, (1969);

[37] S. H. Emerman and R. A. Stephen, *Comment on "Absorbing Boundary Conditions for Acoustic and Elastic Wave Equations" by R. Clayton and B. Engquist*, BSSA 73, (1983), pp 661-665;

[38] Z. S. Alterman and D. Lowenthal, *Seismic Waves in Quarter and Three Quarter Plane*, Geophysics, J. Roy. Astr. Soc. 20, (1970), pp 101-126;

[39] Z. S. Alterman and A. Rotenberg, *Seismic Waves in Quarter Plane*, BSSA 59, (1969), pp 347-368;

[40] D. M. Boore, *Finite Difference Solution to the Equations of Elastic WavePpropagation with Applications to Love Waves Over Dipping Interfaces*, Ph. D. Thesis, M. I. T., (1970);

[41] R. M. Alford, K. R. Kelly and D. M. Boore, *Accuracy of Finite-Difference Modeling by Finite-Difference Methods*, Geophysics 39, (1974), pp 834-842;

[42] R. Stacey, *Improved Transparent Boundary Formulations for the Elastic-Wave Equation*, BSSA 78, (1988), pp 2089-2097;